

GC852  
C6  
no. 256  
ARCHIVE

# DESIGN AND EXECUTION OF THE MARINE STRATOCUMULUS EXPERIMENT

JOSEPH S. WAKEFIELD

WAYNE H. SCHUBERT

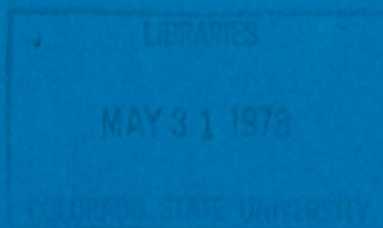


Atmospheric Science

PAPER NO.

256

US ISSN 0067-0340



**DEPARTMENT OF ATMOSPHERIC SCIENCE  
COLORADO STATE UNIVERSITY  
FORT COLLINS, COLORADO**

DESIGN AND EXECUTION OF THE  
MARINE STRATOCUMULUS EXPERIMENT

Joseph S. Wakefield  
Wayne H. Schubert

The research reported here has been supported  
by the GARP Section of the Office of Climate  
Dynamics, National Science Foundation  
Grants ATM 76-09370  
OCD 74-21678,  
by the National Aeronautics and Space Administration  
Grant GA 31588,  
and by the National Center for Atmospheric Research.

Department of Atmospheric Science  
Colorado State University  
Fort Collins, Colorado

September 1976

Atmospheric Science Paper No. 256

## CONTENTS

	Page
FORWARD	iii
ABSTRACT	iv
1.0 INTRODUCTION	1
2.0 DESIGN OF THE MARINE STRATOCUMULUS EXPERIMENT	2
2.1 Review of Lilly's Cloud-Topped Mixed Layer Model	2
2.2 Required Measurements	9
2.3 Aircraft Specifications	10
2.4 Instrumentation on the NCAR Research Aviation Facility Electra	12
2.4.1 Aircraft Position and Winds	20
2.4.2 Air Temperature	22
2.4.3 Water Vapor Content	25
2.4.4 Liquid Water Content	27
2.4.5 Solar and Infrared Radiation	30
2.4.6 Sea Surface Temperature	32
2.4.7 Cloud Condensation Nuclei	32
2.4.8 Cloud Indicators	34
2.4.9 Other Equipment	38
2.5 Base of Operations	40
3.0 FIELD PHASE OF THE MARINE STRATOCUMULUS EXPERIMENT	41
3.1 Flight #1 (05 June 1976)	43
Flight #2 (07 June 1976)	47
Flight #3 (12 June 1976)	51
Flight #4 (13 June 1976)	56
Flight #5 (17 June 1976)	61
3.2 Related Measurements	65
4.0 CONCLUSIONS	68
ACKNOWLEDGEMENTS	69
REFERENCES	70



## ABSTRACT

The design and field phases of an observational program to study marine stratocumulus clouds using a single aircraft (NCAR Electra) are discussed. The basic theoretical framework for the design of the experiment was provided by Lilly's cloud-topped mixed layer model. This theory relates the model unknowns, which are cloud top height, cloud base height, mixed layer moist static energy, mixed layer total water content, and turbulent flux profiles of moist static energy and total water, to certain input parameters, which are sea surface temperature, surface wind speed, large-scale divergence, the temperature and moisture fields above cloud top, and the radiative divergence near cloud top. We attempted to measure all model unknowns and input parameters using the Electra instrumentation and user supplied instrumentation. Five flights off the California coast were made between 5 June and 17 June 1976, each flight lasting approximately six hours. Examples of some of the flight data are shown.

Although most of the flight data remain to be analyzed, our experience in the design and field phases leads us to conclude that much could be gained from a combined meteorological/oceanographic experiment which would include one or two aircraft and an array of three or four ships equipped with oceanographic instrumentation and tethered balloons.

## 1.0 INTRODUCTION

In the strong subsidence regions to the east of the subtropical oceanic high pressure areas there exist large areas of persistent low level stratocumulus clouds. These circulation regimes were first studied observationally by von Ficker (1936) in the eastern Atlantic and by Riehl et al. (1951), Neiburger (1960) and Neiburger et al. (1961) in the eastern North Pacific.

Following this observational work and adopting the modeling philosophy of Ball (1960), Lilly (1968) presented a basic theoretical framework relating the cloud top height, cloud base height, boundary layer temperature and moisture fields, and turbulent flux profiles to the sea surface temperature, large-scale surface wind and divergence, and the temperature and moisture fields above the cloud top. The remarkable insight provided by Lilly's work has stimulated refinements of and experiments with his basic theoretical model (e.g. Deardorff, 1976 and Schubert, 1976). In addition, efforts to incorporate stratocumulus convection in general boundary layer formulations are being made by Randall and Arakawa (see Arakawa, Mintz, et al., 1974) for the UCLA GCM and by Deardorff for the NCAR GCM.

Since the state of stratocumulus theory seemed to be ahead of observational knowledge, a group of us (see the Forward for a list of participants) began designing in the summer of 1975 an observational program using the NCAR Electra. The design of the program is discussed in Chapter 2. The actual flight patterns and some preliminary data are given in Chapter 3. Chapter 4 describes what form a more comprehensive program might take.

## 2.0 DESIGN OF THE MARINE STRATOCUMULUS EXPERIMENT

## 2.1 Review of Lilly's Cloud-Topped Mixed Layer Model

Lilly's cloud-topped mixed layer model (Lilly, 1968) consists of eight equations in the following eight unknowns:

cloud top height	$z_B$
cloud base height	$z_C$
mixed layer moist static energy	$h_M$
mixed layer total water mixing ratio	$(q+\lambda)_M$
turbulent flux of moist static energy at the surface	$(\overline{w'h'})_S$
turbulent flux of moist static energy at the cloud top	$(\overline{w'h'})_B$
turbulent flux of water vapor at the surface	$(\overline{w'q'})_S$
turbulent flux of total water at the cloud top	$\overline{w'(q'+\lambda')}}_B$

All eight unknowns are functions of the horizontal coordinates and time. We shall use a natural coordinate system in which  $x$  denotes distance in the downstream direction. The individual time change  $\frac{d}{dt}$  will then be given by  $\frac{\partial}{\partial t} + V \frac{\partial}{\partial x}$ , where  $V$  is the speed of the horizontal wind. Riehl et al. (1951) and Kraus (1968) have shown that the wind speed and direction over the Eastern North Pacific in summer are nearly constant with height in the lower layers. Thus, we shall assume that there is no turning of the wind with height and no change of wind speed with height. The horizontal projections of all trajectories are then coincident with the surface trajectories. We need not distinguish between horizontal winds at cloud top, in the mixed layer, or at the surface.

With these assumptions the mixed layer budgets of moist static energy and total water are

$$\frac{\partial h_M}{\partial t} + V \frac{\partial h_M}{\partial x} = \frac{(\overline{w'h'})_S - (\overline{w'h'})_B}{z_B}, \quad (1)$$

$$\frac{\partial (q+l)_M}{\partial t} + V \frac{\partial (q+l)_M}{\partial x} = \frac{(\overline{w'q'})_S - \overline{w'(q+l')}_B}{z_B}. \quad (2)$$

These equations state that local changes of  $h_M$  and  $(q+l)_M$  are caused by horizontal advection by the known wind  $V$  and by the vertical convergence of the turbulent fluxes.

Above  $z_B$  the turbulent fluxes jump to zero. Surface turbulent fluxes of  $h$  and  $q$  are given by

$$(\overline{w'h'})_S = C_T V [h_S^* - h_M], \quad (3)$$

$$(\overline{w'q'})_S = C_T V [q_S^* - (q+l)_M]. \quad (4)$$

These equations relate the surface fluxes to the transfer coefficient  $C_T$ , the surface wind speed  $V$ , and the sea-air differences, where  $h_S^*$  and  $q_S^*$  are the saturation values of  $h$  and  $q$  at the sea surface temperature and pressure.

Application of the budget equations for  $h$  and  $q+l$  to the infinitesimally thin layer at the cloud top yields

$$\left( \frac{\partial z_B}{\partial t} + V \frac{\partial z_B}{\partial x} - w_B \right) \Delta h + (\overline{w'h'})_B = \Delta F_R, \quad (5)$$

$$\left( \frac{\partial z_B}{\partial t} + V \frac{\partial z_B}{\partial x} - w_B \right) \Delta(q+\ell) + \overline{w'(q'+\ell')}_B = 0, \quad (6)$$

where  $w_B$  is the large-scale vertical velocity at  $z_B$ ,  $\Delta h$  and  $\Delta(q+\ell)$  are jumps across  $z_B$ , and  $\Delta F_R$  is the jump in the radiative flux across  $z_B$ . These equations are thus the cloud top jump conditions on moist static energy and total water. When multiplied by the density,  $\rho$ , both (5) and (6) contain the quantity  $\rho \left( \frac{\partial z_B}{\partial t} + V \frac{\partial z_B}{\partial x} - w_B \right)$ , which is the net mass flowing into the mixed layer per unit horizontal area per unit time. Such a mass flux into the mixed layer can be due to a local increase in the depth of the mixed layer with time, a horizontal flow across the top of the mixed layer when it deepens in the downstream direction, a large-scale subsidence, or more generally, a combination of these three effects. Non-turbulent air flowing into the mixed layer from above instantaneously changes its moist static energy by an amount  $\Delta h$  and its total water content by an amount  $\Delta(q+\ell)$ , where

$$\Delta h = h(z_B^+) - h_M, \quad (7)$$

$$\Delta(q+\ell) = q(z_B^+) - (q+\ell)_M, \quad (8)$$

$h(z_B^+)$  and  $q(z_B^+)$  being known functions of  $z_B$ . According to (5), the instantaneous change in moist static energy is due to discontinuities in both the turbulent moist static energy flux and the radiative flux, while according to (6), the instantaneous change in total water content is due to a discontinuity in the turbulent total water flux.

Equations (5) and (6) can be regarded as predictive equations for  $z_B$ . In order that they predict  $z_B$  in a consistent manner,

$$\frac{L\Delta(q+\ell)}{\Delta h} (\overline{w'h'})_B - L\overline{w'(q'+\ell')} = \frac{L\Delta(q+\ell)}{\Delta h} \Delta F_R . \quad (9)$$

The cloud base height  $z_C$  is approximately given in terms of the mixed layer total water content  $(q+\ell)_M$  and the saturation mixing ratio just above the surface  $q_0^*$  as

$$z_C = \frac{q_0^* - (q+\ell)_M}{b} = \frac{(1+\gamma) [q_S^* - (q+\ell)_M] - \frac{\gamma}{L} [h_S^* - h_M]}{b} , \quad (10)$$

where  $L$  is the latent heat of condensation,  $b$  is given by

$$b = \frac{g}{C_p} \left( \frac{\partial q}{\partial T} \right)_p + \rho g \left( \frac{\partial q}{\partial p} \right)_T , \quad (11)$$

and  $\gamma$  is defined in (18).

One additional equation is needed to close the system. Lilly has argued that the turbulent energy balance sets maximum and minimum bounds on the entrainment. The entrainment relation,

$$\frac{k}{z_B} \int_0^{z_B} \overline{w's_v'} dz + \frac{1}{2}(1-k)(\overline{w's_v'})_{\min} = 0 , \quad (12)$$

is a weighted average of Lilly's maximum entrainment relation,

$$\int_0^{z_B} \overline{w's_v'} dz = 0 \quad \text{but} \quad \overline{w's_v'} \neq 0 \text{ somewhere,} \quad (13)$$

and his minimum entrainment relation,

$$(\overline{w' s_V'})_{\min} = 0 \quad \text{but} \quad \int_0^{z_B} \overline{w' s_V'} dz > 0 . \quad (14)$$

The weighting factor  $k$  lies between zero and unity. The factor  $\frac{1}{2}$  in the second term of (12) is somewhat arbitrary and has been included so that (12) reduces to the conventional

$$(\overline{w' s_V'})_B = -k (\overline{w' s_V'})_S \quad (15)$$

in the nonsaturated case. Omission of the factor  $\frac{1}{2}$  simply results in a revised interpretation of the parameter  $k$ .

If the effects of both water vapor and liquid water on buoyancy are included in the definition of the virtual dry static energy so that

$$s_V = s + \epsilon L (\delta q - \ell) , \quad (16)$$

then the turbulent virtual dry static energy flux can be expressed as

$$\overline{w' s_V'} = \begin{cases} \beta \overline{w' h'} - \epsilon L \overline{w' (q' + \ell')} & z_C < z < z_B \\ \overline{w' h'} - (1 - \epsilon \delta) L \overline{w' (q' + \ell')} & 0 < z < z_C , \end{cases} \quad (17)$$

where

$$\begin{aligned} \beta &= \frac{1 + \gamma \epsilon (\delta + 1)}{1 + \gamma} & \delta &= 0.608 \\ \epsilon &= \frac{c_p T}{L} & \gamma &= \frac{L}{c_p} \left( \frac{\partial q^*}{\partial T} \right)_p . \end{aligned} \quad (18)$$

Since  $h$  and  $(q+l)$  are constant with height in the mixed layer, their turbulent fluxes must be linear functions of height so that

$$\overline{w'h'} = \left(1 - \frac{z}{z_B}\right)(\overline{w'h'})_S + \frac{z}{z_B} (\overline{w'h'})_B, \quad (19)$$

$$\overline{w'(q'+l')} = \left(1 - \frac{z}{z_B}\right)(\overline{w'q'})_S + \frac{z}{z_B} \overline{w'(q'+l')}_B. \quad (20)$$

Using (17), (19), and (20), the entrainment relation (12) may be written

$$\begin{aligned} & \left[ \beta + (1-\beta) \frac{z_C^2}{z_B^2} \right] (\overline{w'h'})_B + \left[ \beta + (1-\beta) \frac{z_C}{z_B} \left( 2 - \frac{z_C}{z_B} \right) \right] (\overline{w'h'})_S \\ & - \left[ \epsilon + (1-\epsilon(\delta+1)) \frac{z_C^2}{z_B^2} \right] L \overline{w'(q'+l')}_B - \left[ \epsilon + (1-\epsilon(\delta+1)) \frac{z_C}{z_B} \left( 2 - \frac{z_C}{z_B} \right) \right] L (\overline{w'q'})_S \\ & + \frac{1-k}{k} \min \left\{ \begin{array}{l} \beta (\overline{w'h'})_B - \epsilon L \overline{w'(q'+l')}_B \\ \beta \left[ \left( 1 - \frac{z_C}{z_B} \right) (\overline{w'h'})_S + \frac{z_C}{z_B} (\overline{w'h'})_B \right] - \epsilon L \left[ \left( 1 - \frac{z_C}{z_B} \right) (\overline{w'q'})_S + \frac{z_C}{z_B} \overline{w'(q'+l')}_B \right] \\ \left[ \left( 1 - \frac{z_C}{z_B} \right) (\overline{w'h'})_S + \frac{z_C}{z_B} (\overline{w'h'})_B \right] - (1-\epsilon\delta) L \left[ \left( 1 - \frac{z_C}{z_B} \right) (\overline{w'q'})_S + \frac{z_C}{z_B} \overline{w'(q'+l')}_B \right] \\ (\overline{w'h'})_S - (1-\epsilon\delta) L (\overline{w'q'})_S \end{array} \right\} = 0. \end{aligned} \quad (21)$$

Since  $\overline{w's_v'}$  is linear in pressure in the subcloud layer and in the cloud layer but is discontinuous across cloud base, the minimum  $\overline{w's_v'}$  may occur at the top of the cloud layer  $z_B$ , the bottom of the cloud layer  $z_C^+$ , the top of the subcloud layer  $z_C^-$ , or the bottom of the subcloud layer  $z=0$ . These four possibilities for the minimum  $\overline{w's_v'}$  are reflected in the four rows within the large braces of (21).

The purpose of introducing the entrainment condition is to close the system by relating the fluxes at some level above the surface to the fluxes at the surface. Once this is done it becomes possible to compute all the fluxes at all the levels. Only then is the location of the minimum  $\overline{w's_v'}$  known. Thus (21) has a somewhat implicit form.

The theoretical model can now be summarized as follows. In order to determine the eight unknowns listed at the beginning of this section, we use the mixed layer budgets (1) and (2), the surface flux relations (3) and (4), the cloud top jump conditions (5) and (9), the cloud base relation (10), and the entrainment condition (21). These eight equations can be ordered for numerical integration as follows:

$$(\overline{w'h'})_S = C_T V [h_S^* - h_M] , \quad (22)$$

$$(\overline{w'q'})_S = C_T V [q_S^* - (q+l)_M] , \quad (23)$$

$$z_C = \frac{(1+\gamma)[q_S^* - (q+l)_M] - \frac{\gamma}{L} [h_S^* - h_M]}{b} , \quad (24)$$

$$\begin{bmatrix} a_{11} & a_{12} \\ a_{21} & a_{22} \end{bmatrix} \begin{bmatrix} (\overline{w'h'})_B \\ \overline{w'(q'+l')}_B \end{bmatrix} = \begin{bmatrix} b_1 \\ b_2 \end{bmatrix} , \quad (25)$$

$$(26)$$

$$\frac{\partial h_M}{\partial t} + V \frac{\partial h_M}{\partial x} = \frac{(\overline{w'h'})_S - (\overline{w'h'})_B}{z_B}, \quad (27)$$

$$\frac{\partial (q+\ell)_M}{\partial t} + V \frac{\partial (q+\ell)_M}{\partial x} = \frac{(\overline{w'q'})_S - \overline{w'(q'+\ell')}}{z_B}, \quad (28)$$

$$\frac{\partial z_B}{\partial t} + V \frac{\partial z_B}{\partial x} = w_B + \frac{\Delta F_R - (\overline{w'h'})_B}{\Delta h}. \quad (29)$$

Equations (25) and (26) are simply a shorthand notation for (9) and (21). Thus, given initial conditions on  $h_M$ ,  $(q+\ell)_M$  and  $z_B$ , the system (22) - (29) can be numerically integrated. A single computation cycle is as follows:

- i) Compute the surface fluxes  $(\overline{w'h'})_S$  and  $(\overline{w'q'})_S$  from (22) and (23).
- ii) Compute the cloud base  $z_C$  from (24).
- iii) Compute the cloud top fluxes  $(\overline{w'h'})_B$  and  $\overline{w'(q'+\ell')}$  from the two by two system (25) and (26).
- iv) Predict  $h_M$ ,  $(q+\ell)_M$ , and  $z_B$  from (27), (28), and (29), respectively.

## 2.2 Required Measurements

As was discussed in the previous section, Lilly's model relates the properties of the marine stratocumulus layer to the large-scale motion field, the sea surface temperature field, the radiation field and the temperature and moisture fields above the cloud. Thus, given certain inputs the model produces outputs which are measures of the properties

of the marine layer. The inputs and outputs are summarized as follows:

<u>Model Inputs</u>	<u>Model Outputs</u>
sea surface temperature, $T_S$	cloud top height, $z_B$
surface wind speed, $V$	cloud base height, $z_C$
large-scale divergence, $D$	mixed layer moist static energy, $h_M$
radiative divergence near cloud top, $\Delta F_R$	mixed layer total water mixing ratio, $(q+\ell)_M$
moist static energy above the mixed layer, $h(z_B^+)$	profiles of the turbulent fluxes of moist static energy, $\overline{w'h'}$ and total water, $\overline{w'(q'+\ell')}$
water vapor mixing ratio above the mixed layer, $q(z_B^+)$	

Our intention was to measure all model input and output quantities as functions of distance in the downstream direction and as functions of time of day. Variations in the downstream direction reveal how the properties of the mixed layer are modified as the air flows toward the ITCZ. Variations with the time of day reveal how the mixed layer responds to diurnally varying radiation off the cloud top. The required measurements and instrumentation are summarized in Table I.

### 2.3 Aircraft Specifications

The aircraft chosen for the marine stratocumulus experiment was a Lockheed Electra (Model L-188C) leased by the National Center for Atmospheric Research<sup>1</sup>, Boulder, Colorado. The Electra was chosen both for

<sup>1</sup> NCAR is sponsored by the National Science Foundation.

TABLE I. REQUIRED MEASUREMENTS

<u>Parameter</u>	<u>Instrumentation</u>
1) sea surface temperature, $T_S$	PRT - 5
2) surface wind speed, $V$	gust probe/INS
3) large-scale divergence, $D$	apparently too small to accurately measure
4) radiative divergence near cloud top, $\Delta F_R$	upward and downward looking pyranometers and pyrgeometers
5) moist static energy above the mixed layer, $h(z_B^+)$	resistance wires, hygrometers
6) water vapor mixing ratio above the mixed layer, $q(z_B^+)$	hygrometers
7) cloud top height, $z_B$	pressure altimeter, wet bulb thermistor, nephelometer, lidar
8) cloud base height, $z_C$	pressure altimeter, wet bulb thermistor, nephelometer, lidar
9) mixed layer moist static energy, $h_M$	resistance wires, hygrometers, wet bulb thermistor
10) mixed layer total water mixing ratio, $(q+\ell)_M$	hygrometers, wet bulb thermistor, liquid water meters, PMS-Knollenberg probes
11) profile of turbulent flux of moist static energy, $\frac{w'h'}{w'h'}$	gust probe/INS for $w'$ ; for $h'$ below $z_C$ resistance wires, hygrometers; for $h'$ above $z_C$ wet bulb thermistor, PRT-6.
12) profile of turbulent flux of total water $w'(q'+\ell')$	gust probe/INS for $w'$ ; for $q'$ below $z_C$ hygrometers; for $q'$ above $z_C$ wet bulb thermistor, PRT-6; for $\ell'$ above $z_C$ liquid water meters, PMS-Knollenberg probes.
13) remote measurement of cloud top	lidar

its instrumentation and for its range. It is shown in Fig. 1.

The Electra's fuel capacity is sufficient to allow a six to seven hour low-level experimental flight. Specifications and performance are given in Table II.

Flight duty limitations for the crew, as set down by the Research Aviation Facility of NCAR (Burris, 1975) are listed in Table III.

#### 2.4 Instrumentation on the NCAR Research Aviation Facility Electra

Data recording, real-time computations, and meteorological and flight data display are performed by the NCAR Electra Data Management System (Kelley, 1973a; Duncan, 1973). The system serves as a low-noise data recorder, with input flexibility provided by software control. Most of the data are recorded at 10 Hz, so turbulence measurements are possible.

Real-time derived meteorological and flight data may be displayed on any of six television monitors located throughout the aircraft (Fig. 2). In addition, analog voltages for eight parameters are available for strip chart display (Fig. 3). At the start of the marine stratocumulus experiment, the parameters recorded on the strip chart were wind direction, wind speed, wet-bulb thermistor temperature, air temperature, dew point temperature, pressure altitude, equivalent potential temperature, and time. Time marks may be placed in the digital data record from any of several stations located throughout the aircraft.

The Electra's instrumentation is discussed in the following sections. RAF-supplied instrumentation specifications are listed in Table IV.



Fig. 1. NCAR Electra at Ames Research Center, Moffet Naval Air Station, Mountain View, California.

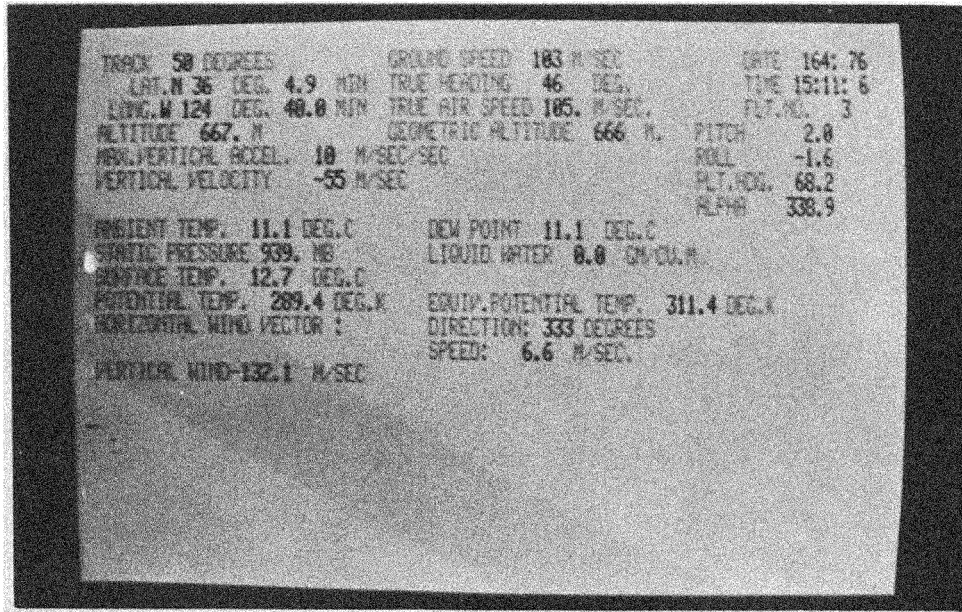


Fig. 2. Television monitor displaying real-time derived meteorological and flight data.

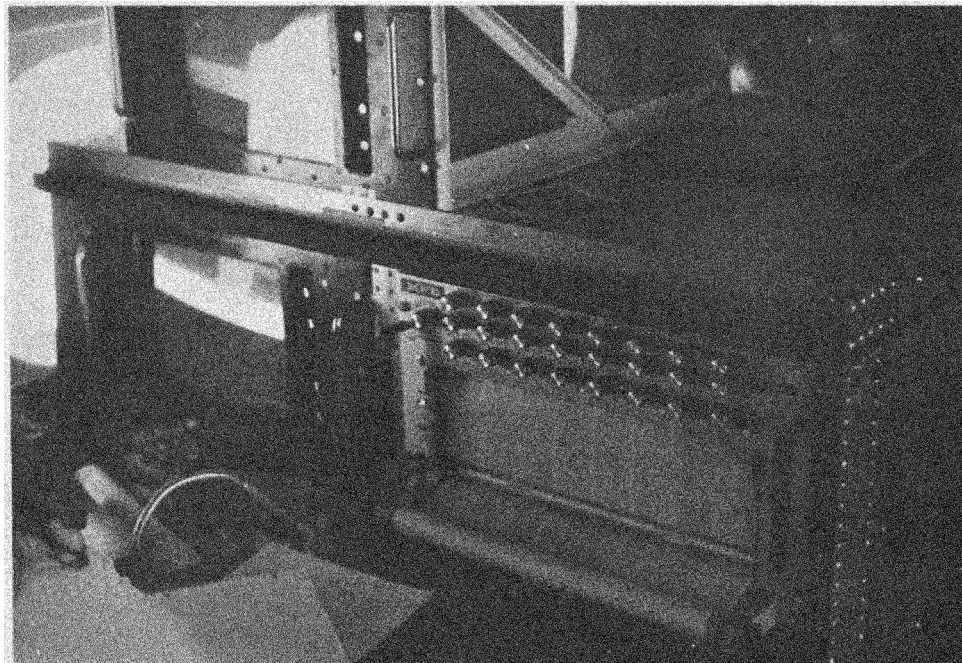


Fig. 3. Television monitors (left) and eight parameter strip chart (right).

TABLE IIa. ELECTRA L-188C SPECIFICATIONS

Engine Power:	11 186 kW (15 000 hp)
Wingspan:	30 m (99 ft)
Length:	32 m (105 ft)
Cabin Floor Area:	58 m <sup>2</sup> (628 ft <sup>2</sup> )
Empty Mass:	26 650 kg (58 700 lb)
Maximum Gross Mass:	52 665 kg (116 000 lb)
Maximum Payload Mass:	12 020 kg (26 500 lb)
Maximum Landing Mass:	43 385 kg (95 650 lb)
Research Electrical Power:	60 kVA
Fuel Capacity:	24 678 l (6520 gal) usable fuel

TABLE IIb. ELECTRA PERFORMANCE

Maximum speed at 3700 m:	200 ms <sup>-1</sup>
Cruising speed at 39 000 kg (85 500 lb) at 6700 m:	180 ms <sup>-1</sup>
Service ceiling at 45 000 kg (100 000 lb):	8700 m
Slow flight speed:	IAS 60 ms <sup>-1</sup>
FAA takeoff runway at 51 000 kg (113 000 lb) sea level standard day:	1440 m (4720 ft)
Maximum operating altitude:	9150 m

TABLE IIc. PERFORMANCE AT RESEARCH GROSS MASS

<u>ALTITUDE (m)</u>	<u>RANGE (km)</u>	<u>TIME (h:min)</u>
7000	5450	9:09
3000	4250	7:39
150	3470	6:35

TABLE III. ELECTRA CREW DUTY LIMITATIONS

## Flight time limitations:

Daily: 9 h

Weekly: 35 h

Monthly: 110 h

Consecutive working days: Maximum of six

Maximum crew duty period: 14 h

Minimum crew rest: 12 h between duty periods

TABLE IV. AIRCRAFT INSTRUMENTATION

Parameter Measured	Instrument Type	Manufacturer & Model No.	Combined Performance of Transducer, Signal Conditioning, and Recording:				
			Range	Accuracy	Time Constant#	Precision	Resolution
Aircraft Pitch & Roll Angles	Inertial Nav. Resolver	Litton APD 917055	±45°	±0.008°	0.016 s	--	0.005°
Inertial Platform Hdg.	Inertial Nav. Resolver	Litton APD 917055	±45°	±0.05°	0.016 s	--	0.005°
Aircraft Ground Speed	Inertial Nav. System	Litton LTN-51	0 to 400 ms <sup>-1</sup>	±1 ms <sup>-1</sup> *	0.032 s	--	0.04 ms <sup>-1</sup>
Aircraft Vertical Vel.	Inertial Nav. System	Litton LTN-51	±50 ms <sup>-1</sup>	±0.10 ms <sup>-1</sup>	0.016 s	--	0.012 ms <sup>-1</sup>
Aircraft True Heading & Inertial Wander Angle	Inertial Nav. System	Litton LTN-51	0 to 360°	±0.05°	0.064 s	--	0.001°
Aircraft Latitude	Inertial Nav. System	Litton LTN-51	±90°	±0.066°	1 s	--	0.001°
Aircraft Longitude	Inertial Nav. System	Litton LTN-51	±180°	±0.066°	1 s	--	0.001°
Angles of Attack and Sideslip	Fixed Vane (Strain gage)	NCAR Development	±10°	±0.5°	0.016 s	--	0.005°
	Rotating Vane (LVDT)	NCAR Development	±10°	±0.5°	0.016 s	--	0.002°

# Time constants are generally determined by the data system.

\* The indicated values are means for flights of four hour durations, longer flights will result in degraded accuracy without external update.

TABLE IV. AIRCRAFT INSTRUMENTATION

Continued

Parameter Measured	Instrument Type	Manufacturer & Model No.	Combined Performance of Transducer, Signal Conditioning, and Recording:				
			Range	Accuracy	Time Constant	Precision	Resolution
Geometric Altitude	Radio Altimeter	Sperry Rand AA-220	0 to 762 m	$\pm 1.5$ m, 0-30 m $\pm 8$ m, 30-150 m $\pm 53$ m, 150-762 m	0.16 s	--	0.19 m
Pressure Altitude	Variable Capacitance	Rosemount Engr. Co. 1301-A	300 to 1035 hPa	$\pm 1$ hPa	0.16 s	$\pm 0.5$ hPa	0.09 hPa
Indicated Airspeed	Variable Capacitance	Rosemount Engr. Co. 1301-B	0 to 150 $\text{ms}^{-1}$	$\pm 0.2$ $\text{ms}^{-1}$	0.16 s	$\pm 0.2$ $\text{ms}^{-1}$	0.03 $\text{ms}^{-1}$
	Variable Reluctance	Tavis P-1	0 to 125 $\text{ms}^{-1}$	$\pm 0.2$ $\text{ms}^{-1}$	0.016 s	--	0.03 $\text{ms}^{-1}$
Total Air Temperature	Platinum Resistance	Rosemount Engr. Co. 102E2AL	-60 to +40°C	$\pm 0.2$ °C	0.16 s	$\pm 0.2$ °C	0.02°C
	1 meter Tungsten Wire	NCAR Development	-60 to +50°C	$\pm 1.0$ °C	0.016 s	$\pm 0.3$ °C	0.03°C
	Wet Bulb Thermistor	NCAR Development	--	--	--	--	--
Water Vapor Content	Thermoelectric Hygrometer	EG&G 137-C3-S3	-50 to +50°C	$\pm 0.5$ °C, >0°C $\pm 1.0$ °C, <0°C	0.32 s	$\pm 0.1$ °C	0.01°C
	Lyman-Alpha Hygrometer	NCAR Development	0 to 40 $\text{g kg}^{-1}$	--	0.05 s	--	0.01 $\text{g kg}^{-1}$
	Microwave Refractometer	National Bureau of Standards	0 to 300 N	--	0.016 s	--	0.037 N

TABLE IV. AIRCRAFT INSTRUMENTATION

Continued

Parameter Measured	Instrument Type	Manufacturer & Model No.	Combined Performance of Transducer, Signal Conditioning, and Recording:				
			Range	Accuracy	Time Constant	Precision	Resolution
Cloud Liquid Water Content	Laser Spectrometer	Particle Measuring Systems	20 to 300 $\mu\text{m}$	--	1 s	--	20 $\mu\text{m}$
	Hot-wire Flowmeter	Johnson-Williams LWH	0 to 6 $\text{gm}^{-3}$	--	1.5 s	--	0.001 $\text{gm}^{-3}$
Radiation	Pyrgeometer 4 to 45 $\mu\text{m}$	Eppley PIR	0 to 1750 $\text{Wm}^{-2}$ *	--	1 s	--	4.2 $\text{Wm}^{-2}$
	Pyranometer 285 to 2800 nm	Eppley 2-WG7	0 to 1750 $\text{Wm}^{-2}$ *	--	1 s	--	4.2 $\text{Wm}^{-2}$
	Pyranometer 285 to 1530 nm	Eppley 2-0G1	0 to 1750 $\text{Wm}^{-2}$ *	--	1 s	--	4.2 $\text{Wm}^{-2}$
	Pyranometer 285 to 700 nm	Eppley 2-RG8	0 to 1750 $\text{Wm}^{-2}$ *	--	1 s	--	4.2 $\text{Wm}^{-2}$
Sea Surface Temperature	Bolometric Radiometer	Barnes Engr. Co PRT-5	-20 to +75°C	$\pm 0.5^\circ\text{C}$	0.16 s	--	0.01°C

\* Range and Resolution Variable

#### 2.4.1 Aircraft Position and Winds

INERTIAL NAVIGATION SYSTEM (Leondes, 1970; Lenschow, 1972)

A Litton Industries model LTN-51 Inertial Navigation System (INS) is mounted inside the base of the Electra noseboom, just forward of the nose of the aircraft.

An INS consists basically of three orthogonally mounted gyroscopes, three orthogonally mounted accelerometers, and a digital computer. The gyroscopes keep the reference platform stable and the accelerometers sense changes in the platform's inertia. The computer integrates the output of each accelerometer and computes the velocity and position of the aircraft. Short term accuracy (<2 minutes) is  $\pm 0.1 \text{ ms}^{-1}$ . Long term accuracy is  $\pm(1.0 + 0.5t) \text{ ms}^{-1}$ , where  $t$  is in hours.

Meteorological applications of inertial navigation may be found in Axford (1968), Lilly and Lenschow (1971), Kelley (1973b), Lenschow (1973a), Pennell and LeMone (1974), Telford and Wagner (1974), and LeMone and Pennell (1976).

GUST PROBE (Lenschow, 1971, 1972, 1973b, 1975)

The gust probe is mounted on a boom 5.6 m ahead of the nose of the Electra. It consists of four vanes, two each for angle of attack and angle of sideslip, and a pitot tube (see Fig. 4). One of each pair of vanes is free to rotate and align itself with the airstream. Its angle is then obtained directly from the output of an angle transducer. The other vane of the pair is constrained from rotating, the force on the vane being determined by strain gauges mounted in the base of the vane. The incidence angle is directly proportional to the force and inversely

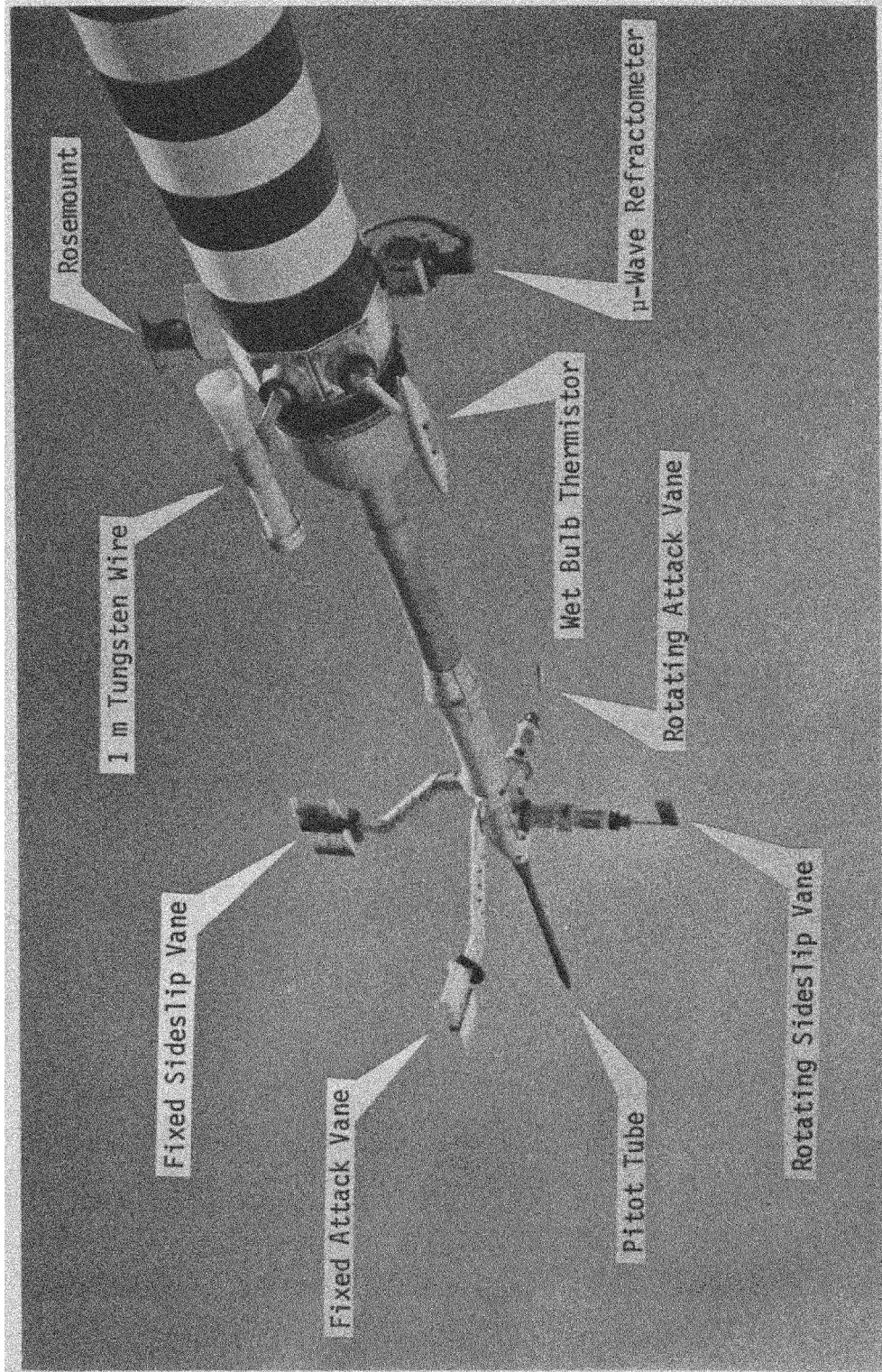


Fig. 4. Electra nose boom.

proportional to the vane area and the pitot-static pressure. The pitot tube is used to measure the fluctuations of the along-axis wind.

## ALTIMETERS

The Electra is also equipped with a radio altimeter, which is usable up to 792 m and is accurate to about 7%. The usual complement of pressure altimeters and airspeed indicators is also present.

### 2.4.2 Air Temperature

ROSEMOUNT TOTAL TEMPERATURE PROBE (DeLeo and Werner, 1960; Lenschow, 1972; Lenschow and Pennell, 1974)

One of the Electra's two Rosemount platinum resistance total temperature probes is shown in Fig. 4. The other is mounted on the fuselage. A schematic drawing of the probe is shown in Fig. 5. The probe is designed such that the air turns a 90° corner and is decelerated adiabatically before contacting the 27 cm wound sensing element. This corner is intended to prevent cloud droplets or other aerosols from impacting on the wire and causing breakage or wet bulbing. This is more successful from the non-breakage point of view as droplets sufficient to wet the element apparently negotiate the bend when flying in clouds, unless the clouds have low liquid water contents (Lenschow and Pennell, 1974).

The Rosemount probe is a fast-response instrument with a time constant of approximately 1/6 second.

ONE METER TUNGSTEN WIRE (Lenschow, 1972; Lenschow and Pennell, 1974)

This probe is shown in Fig. 4. It consists of a 1 m tungsten wire

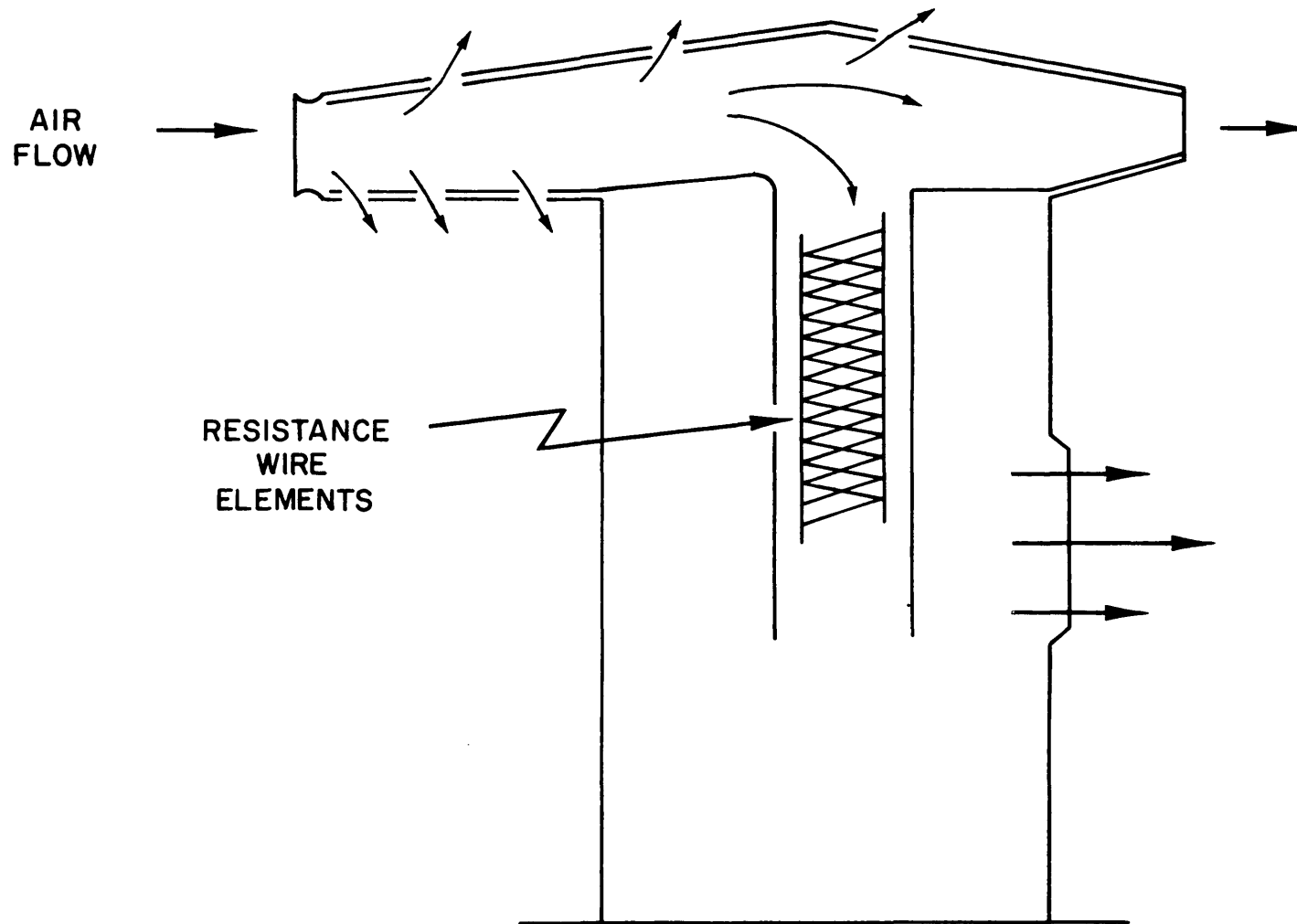


Fig. 5. Schematic drawing of Rosemount total temperature probe.

exposed more directly to the air flow than is the Rosemount. As a result, it becomes wet rapidly in cloud, but is very fast in response, having a time constant of 1/60 sec.

#### WET BULB THERMISTOR (Lenschow and Pennell, 1974)

This instrument, which was designed and built at NCAR by D. Lenschow and K. Danninger, is shown in Fig. 4. A bead thermistor is covered with lint and exposed to the air stream. It thus serves as a dry bulb outside of clouds and a wet bulb inside of clouds, since the lint is rapidly moistened in clouds. The thermistor, due to its small size, has a fast response time, and is therefore good for turbulence studies. Being small, however, means that it is very fragile and cannot be flown in precipitation.

The wet bulb thermistor was installed as an experimental instrument on these flights. Preliminary results indicate that it worked well.

#### PRT-6 RADIOMETER (Barnes Engineering Company, 1971)

A Barnes Engineering Company model PRT-6 radiometer was loaned by S. K. Cox of Colorado State University and operated by B. A. Albrecht and K. T. Griffith of C. S. U. It operates by comparing the energy emitted by the target source with that emitted by a cavity of known reference temperature. A three-blade chopper operating at 33 1/3 Hz yields a 100 Hz source/reference comparison.

For this experiment, the radiometer was operated with a 2° field of view, and was filtered for the CO<sub>2</sub> band around 14 μm. The purpose was to use it as a thermometer for cloud temperature measurements. Initial data indicate that the output is highly roll dependent, except when within a cloud to a sufficient depth that the optical depth has been exceeded.

### 2.4.3 Water Vapor Content

THERMOELECTRIC DEW POINT HYGROMETER (E. G. & G., Inc., Waltham, Massachusetts)

A pair of these hygrometers are mounted on the Electra, one on each side of the fuselage near the nose of the aircraft. The instrument works on the principle of detecting the changes in reflected and scattered light off of a mirror, upon deposition of a condensate. The mirror is cooled thermoelectrically until dew forms on its surface. The mirror is then heated in order to evaporate the dew to a very thin layer, where the instrument stabilizes. The temperature of the mirror at that time is thus the dew point temperature. A similar instrument is described by Francisco and Beaubien (1965).

Such an instrument is not very fast in response, but its long term accuracy allows it to be used as a reference for faster responding but less stable instruments.

LYMAN- $\alpha$  HYGROMETER (Buck, 1975)

The operating principle of this instrument is the absorption of the Lyman- $\alpha$  line (121.56 nm) by water vapor. Beer's law states that, ideally, the absorption of a single line is exponential:

$$I = I_0 e^{-k\rho x} ,$$

where  $I$  and  $I_0$  are received and transmitted intensity (collimated source),  $k$  is an absorption coefficient,  $\rho$  is absorber concentration, and  $x$  is the path length. The ideal is complicated by impurities and drift.

The NCAR instrument compensates for impurities by using a specially-designed high-purity source, and drift may be accounted for by comparison with other instruments.

The NCAR Lyman- $\alpha$  hygrometer has a time constant of 1/20 second.

#### MICROWAVE REFRACTOMETER (Thomson, 1972)

Atmospheric radio "refractivity" is a function of pressure, temperature, and water vapor pressure, primarily. If effects of carbon dioxide and other trace atmospheric constituents are considered constant, then an empirically-derived formula for atmospheric radio "refractivity" may be written as

$$N \equiv (n-1) \times 10^6 = \frac{77.6}{T} \left( p + 4810 \frac{e}{T} \right),$$

where  $n$  is the radio refractive index,  $N$  is in "N units", a conveniently scaled quantity,  $T$  is temperature in Kelvin,  $p$  is the total pressure, and  $e$  is the partial pressure of water vapor, in hectopascals (the hectopascal is equivalent to the millibar).

Consequently,  $e$  may be determined by measuring  $N$ ,  $p$ , and  $T$ , and applying the formula

$$e = \left( \frac{NT}{77.6} - p \right) \frac{T}{4810}$$

In the microwave refractometer (Fig. 4) the resonant frequency of a reference cavity is compared to that of a sample cavity, the time variation of this resonant frequency difference being a measure of the time variation of the "refractivity"  $N$ . Using the time series of  $N$ ,  $T$ , and  $p$ , a time series of  $e$  can be derived.

#### 2.4.4 Liquid Water Content

FORWARD SCATTERING SPECTROMETER PROBE (Particle Measuring Systems, 1975, 1976)

The FSSP was supplied by Particle Measuring Systems, Inc. and operated by R. Knollenberg and J. Knollenberg. It is shown mounted on the Electra in Fig. 6. The operating and data systems are shown in Fig. 7.

The FSSP will detect and size particles ranging in diameter from 0.5  $\mu\text{m}$  to 45  $\mu\text{m}$  in four ranges: 0.5 to 7.5  $\mu$ ; 1-15  $\mu$ ; 2-30  $\mu$ ; and 3-45  $\mu$ . Each size range is divided into 15 channels.

A rough sketch illustrating the principle of operation is shown in Fig. 8. The sample volume is illuminated by a laser. Light scattered by any particles present bypasses the dump spot and reaches the detector. The amount of light reaching the detector is proportional to the size of the particle.

Concentrations observed during this experiment were in the range of 150 to 200  $\text{cm}^{-3}$ . Coincidence errors at such levels are approximately 1%. At concentrations of 1000  $\text{cm}^{-3}$  (as are common in deep Cu and Cbs), coincidence errors approach 10%.

OPTICAL ARRAY PROBE (Knollenberg, 1970, 1972; Particle Measuring Systems, 1975)

The principle of operation of this device (see Fig. 6) is simple and is shown schematically in Fig. 9. As a particle passes through a collimated light beam, it casts a shadow, which is then magnified and cast upon an array of photodiodes. The number of these photodiodes occulted is thus proportional to the diameter of the particle. The probe used in the present



Fig. 6. Knollenberg Forward Scattering Spectrometer Probe (left) and Optical Array Probe (right).

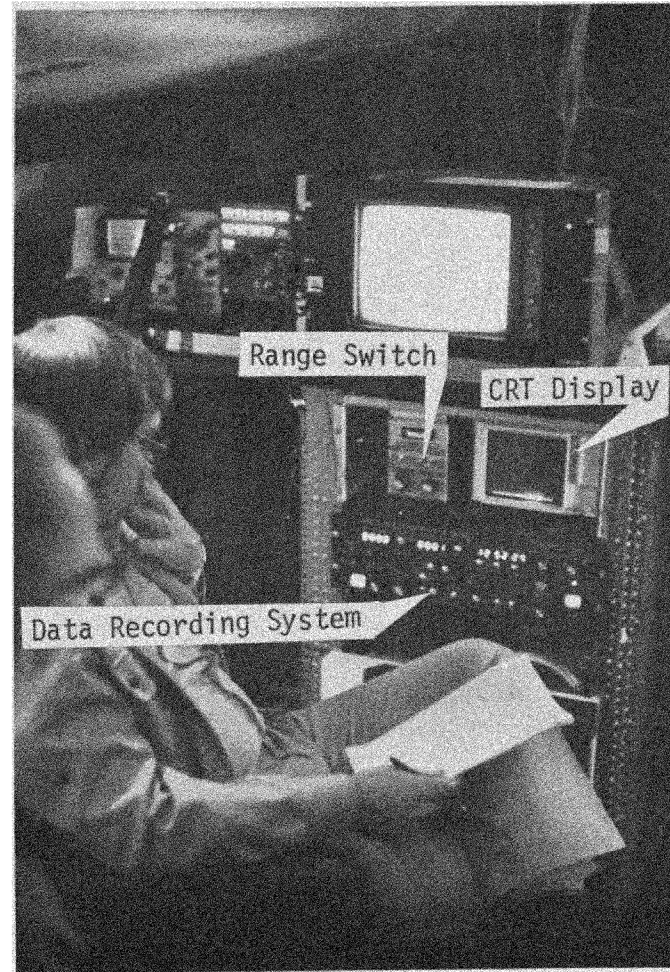


Fig. 7. Operating and data systems for Knollenberg FSSP.

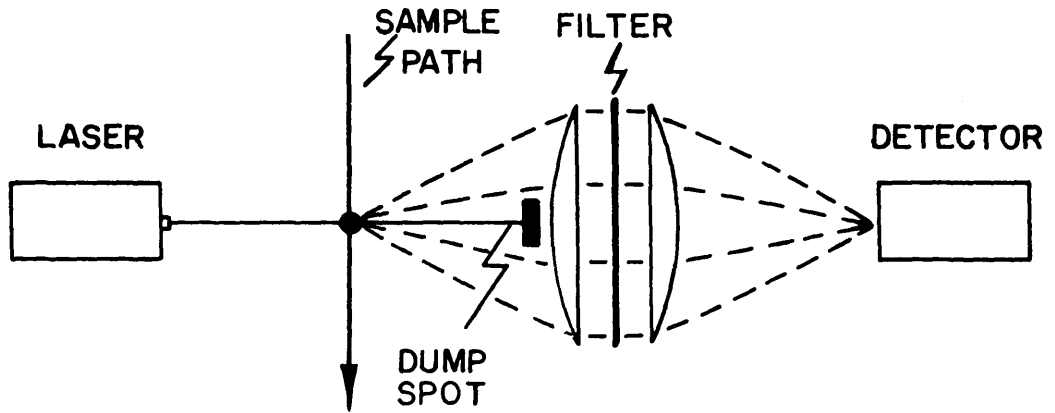


Fig. 8. Principle of operation of the Knollenberg FSSP.

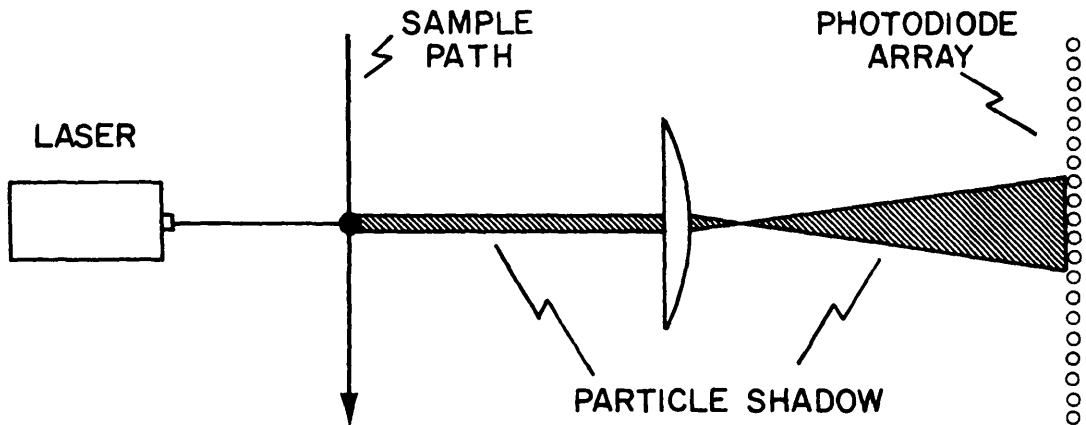


Fig. 9. Principle of operation of the Knollenberg OAP.

experiment has an array with 24 elements, capable of sizing particles from 20  $\mu\text{m}$  to 300  $\mu\text{m}$  diameters, in fifteen 20  $\mu$  channels.

#### ELECTROSTATIC DISDROMETER (Abbott et al., 1972; Dye, 1976)

J. Doyne Sartor of NCAR supplied the disdrometer and handled its operation on the research flights.

The disdrometer (shown in the photo in Fig. 10) detects cloud droplets by sensing the charge removed from an electrode by the droplets. Air is drawn through a hole at the end of the probe. Inside, any droplets present break up and the fragments impact upon a hemispherical electrode. The size of the incident droplet is determined from the amplitude of the observed voltage drop.

#### JOHNSON-WILLIAMS HOT WIRE DEVICE (Neel and Steinmetz, 1952; Neel, 1955; see also Knollenberg, 1972; Ruskin, 1976)

This device consists of a heated wire with a known temperature coefficient of resistance. The wire is connected in a bridge circuit, and water droplets impinging on it cause a loss of heat. The resulting change in resistance is related to the amount of liquid water in the airstream.

The hot wire meter is useful for cloud liquid water measurements, but due to droplet size limitations, it will not work for precipitation. On the present experiment, however, this was not a problem, since we did not expect to encounter precipitating clouds.

#### 2.4.5 Solar and Infrared Radiation

The Electra is equipped with two radiometer pods, one upward-looking

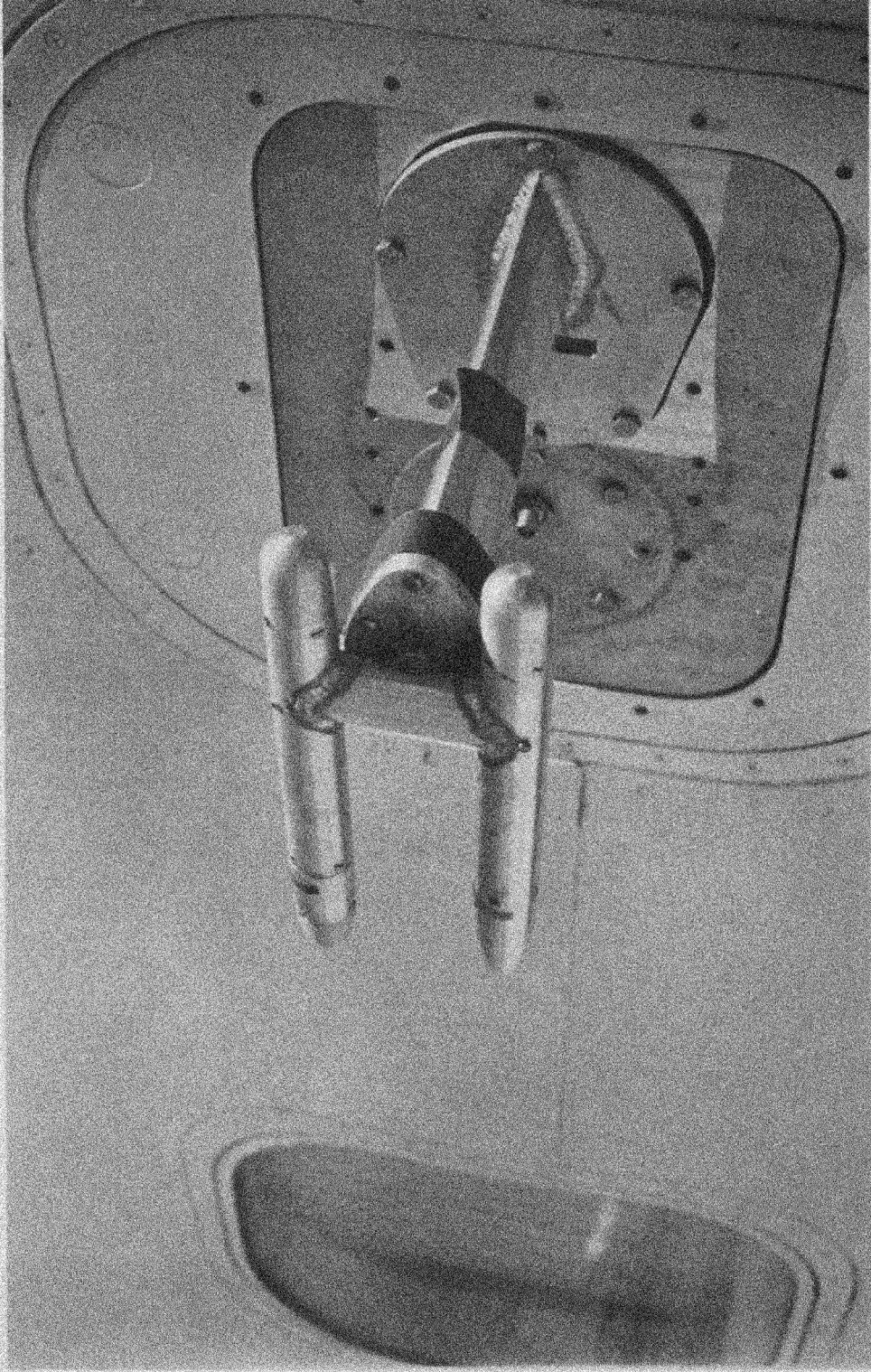


Fig. 10. Electrostatic disdrometer probes.

and the other downward-looking. Each holds four radiation instruments. These consist of upward- and downward-looking pyranometers (six) and pyrgeometers (two). The pods are retractable for ferry flight periods, to avoid unnecessary damage to or soiling of instrument domes.

The Eppley Laboratory pyranometers and pyrgeometers are designed to measure hemispherical radiation. The pyranometers measure radiation with wavelengths of 285 to 2800 nm, in various ranges (see Table IV). The pyrgeometers are sensitive in the 4 to 45  $\mu\text{m}$  range. Each of the Eppley instruments has as its sensor a multi-junction thermopile, whose output is related to the received radiation. Further information may be found in Eppley Laboratory (1971), Albrecht et al. (1973), and Albrecht and Cox (1976).

#### 2.4.6 Sea Surface Temperature

Sea surface temperature was determined by measuring infrared radiation with a Barnes Engineering Company Model PRT-5 radiometer. The PRT-5 is identical in operation to the PRT-6 described earlier (section 2.4.2). It is sensitive in the 9.5 to 11.5  $\mu\text{m}$  spectral range, and has a claimed accuracy of  $\pm 0.5^\circ\text{C}$  over a range of  $-20^\circ\text{C}$  to  $+75^\circ\text{C}$ .

#### 2.4.7 Cloud Condensation Nuclei

The Cloud Condensation Nuclei Spectrometer (Fukuta et al., 1974; Saxena and Fukuta, 1976) was supplied and operated by V. K. Saxena and R. Nye of the Denver Research Institute of the University of Denver. The photo (Fig. 11) shows some of its external features.

The spectrometer consists of two parallel copper plates. The plates

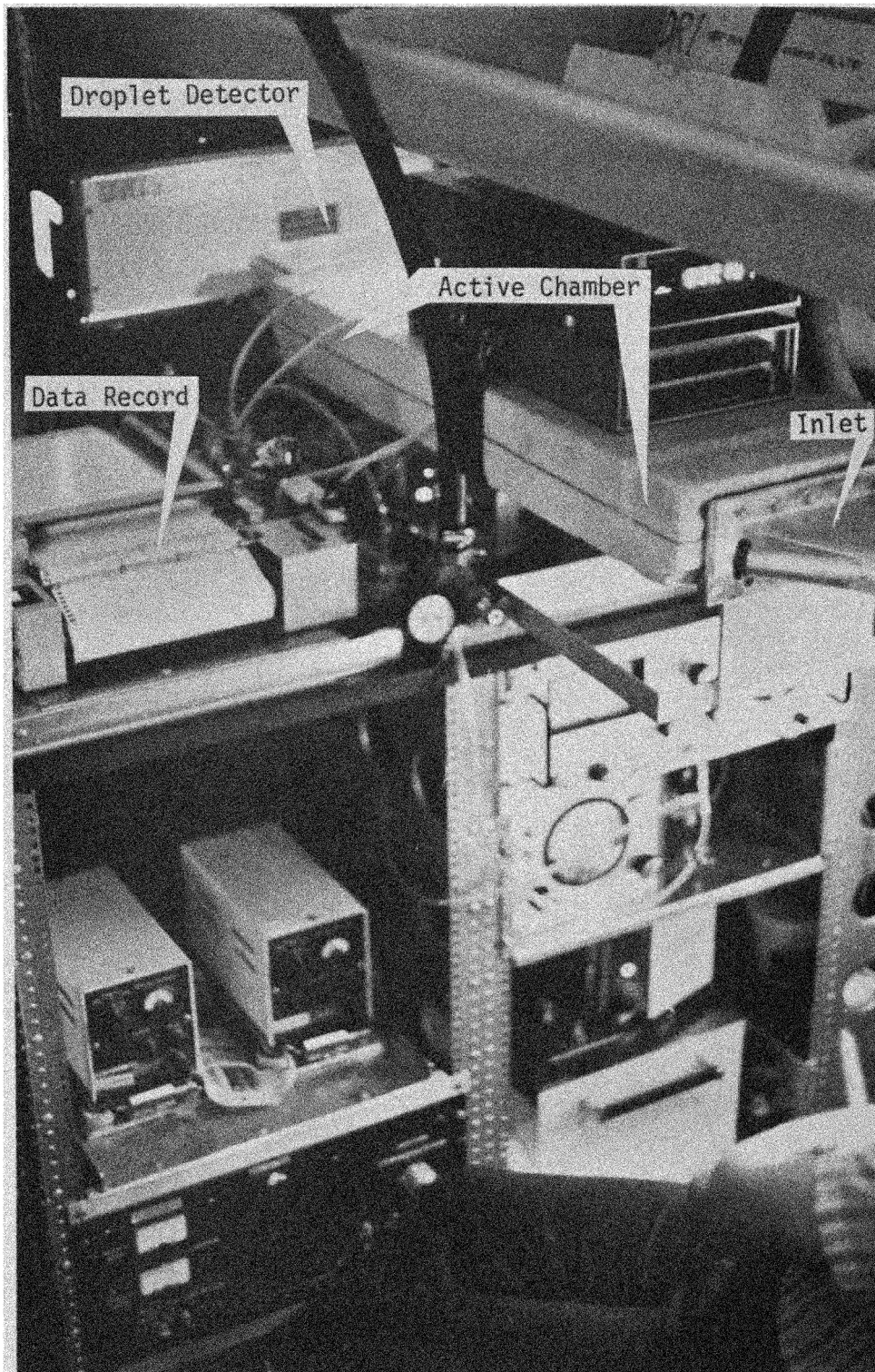


Fig. 11. Cloud Condensation Nuclei (CCN) Spectrometer.

are joined together on one edge by a heat conducting material, and on the other edge by a non-conducting material, as shown in Fig. 12. A temperature difference is created by heating the top plate to temperature  $T_2$  and cooling the bottom plate to temperature  $T_1$  along the edges joined by the insulator. In the steady state, the temperature profiles are linear in the vertical, and also in the horizontal along each plate. The temperature along the median plane (shown by the dashed line in the figure) is constant at  $(T_2 + T_1)/2$ . The supersaturation achievable in a steady-state situation such as this is dependent upon the magnitude of the vertical temperature difference. Thus the supersaturation which occurs along the median plane is greatest near the nonconducting wall and decreases toward the conducting wall.

Water vapor is supplied to the sample air by moist filter papers placed underneath the top plate and atop the bottom plate. The upper filter paper is shaped to allow droplets to reach a uniform size for sampling, regardless of supersaturation, as shown in Fig. 13. This configuration allows droplets to grow longer at lower supersaturation. An optical scan is made across the exit end of the spectrometer, so activation as a function of supersaturation may be determined.

The data are recorded both on an x-y plotter for real-time analysis and on the Electra Data Management System.

#### 2.4.8 Cloud Indicators

LIDAR (Grams and Wyman, 1972; Grams, 1974-75; Grams et al., 1975)

The lidar (or laser radar) system presently in use was developed specifically for the Electra by G. W. Grams and C. M. Wyman of NCAR.

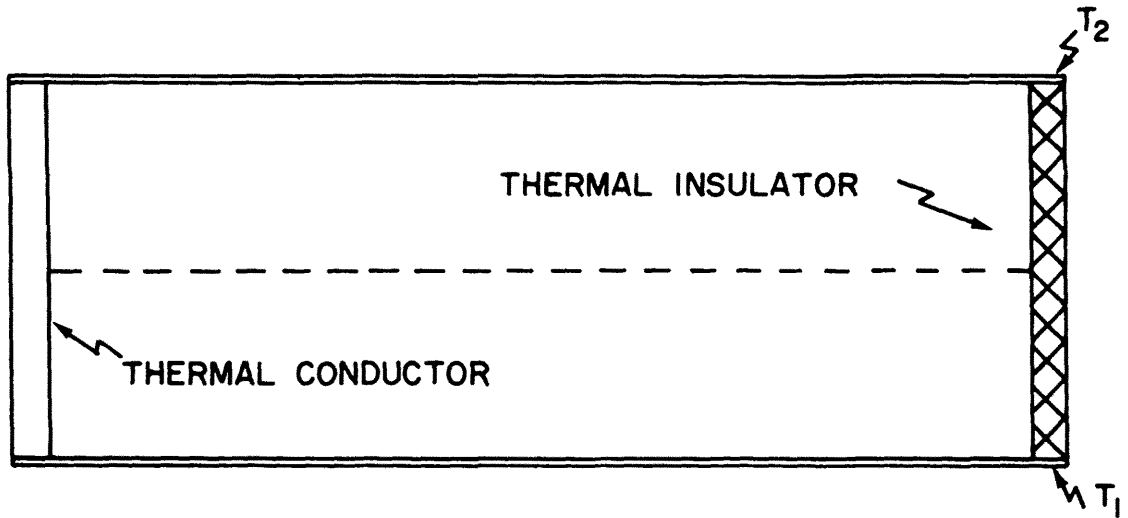


Fig. 12. Cross section of active chamber of CCN Spectrometer.

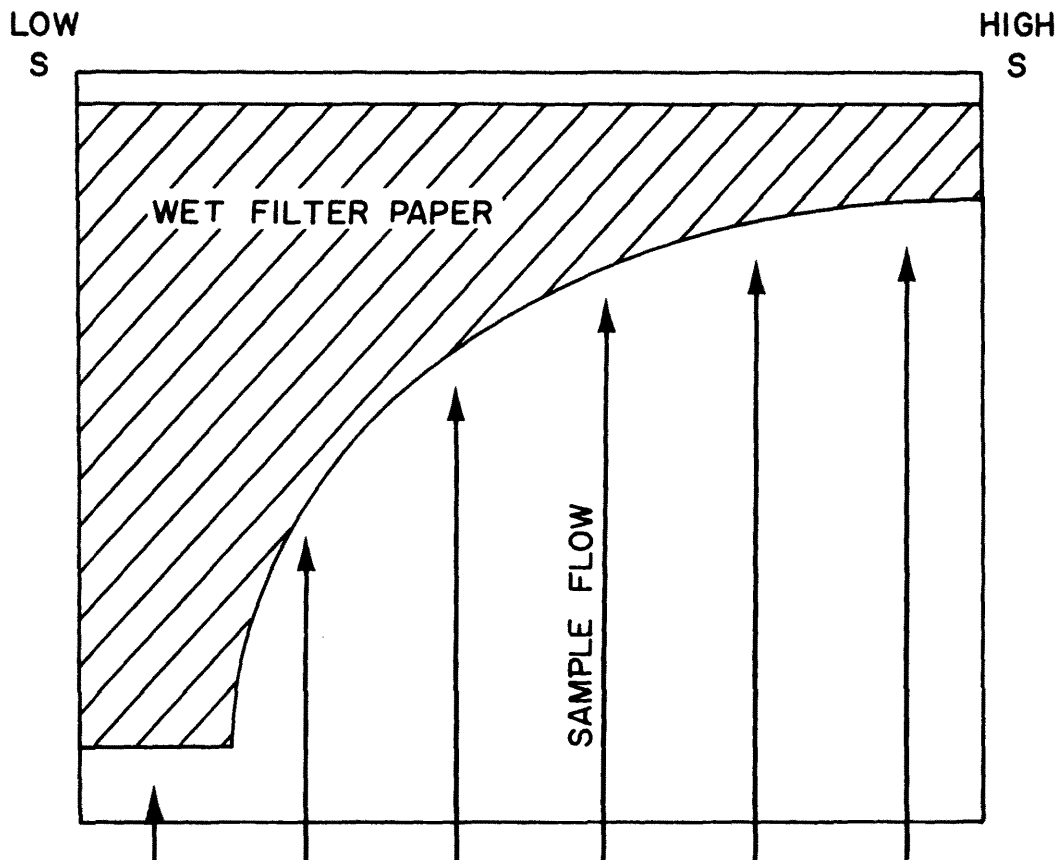


Fig. 13. Top view of active chamber of CCN Spectrometer.

The system consists of a pulsed dye laser, a Cassegrain telescope, and analyzing and recording electronics. Figures 14 and 15 are photographs of the lidar system as installed in the Electra.

The laser was pulsed every 3 to 4 seconds at a wavelength of 585 nm. Returning signals were integrated over 200 ns intervals, giving a spatial resolution of 30 m in the vertical. The first detectable signal comes from 30-50 m away from the aircraft. The system includes a rotatable mirror which allows either upward- or downward-looking operation.

An on-line computer provides real-time analysis of signal received vs. height as well as magnetic tape recording for post-analysis.

The purpose of the lidar on this experiment was twofold. First, it was intended to give a quantitative measure of how far below cloud base (in upward-looking mode) or how far above cloud top (downward-looking) the aircraft was at any time. This would allow data to be stratified according to those parameters, as well as give quantitative information about cloud top and cloud base height. Second, the lidar was intended to provide for stratification of data between cloud and no-cloud overhead situations.

#### FIXED ANGLE NEPHELOMETER

The nephelometer, like the lidar, was built and operated by G. W. Grams and C. M. Wyman of NCAR. The nephelometer may best be described as a "mini-lidar". A diagram is shown in Fig. 16. An infrared LED provides the signal, whose backscatter from a region 3-4 m outside of the aircraft window is detected. Thus, the nephelometer may serve as a cloud/no-cloud indicator. The LED signal is oscillatory, to allow for the removal of

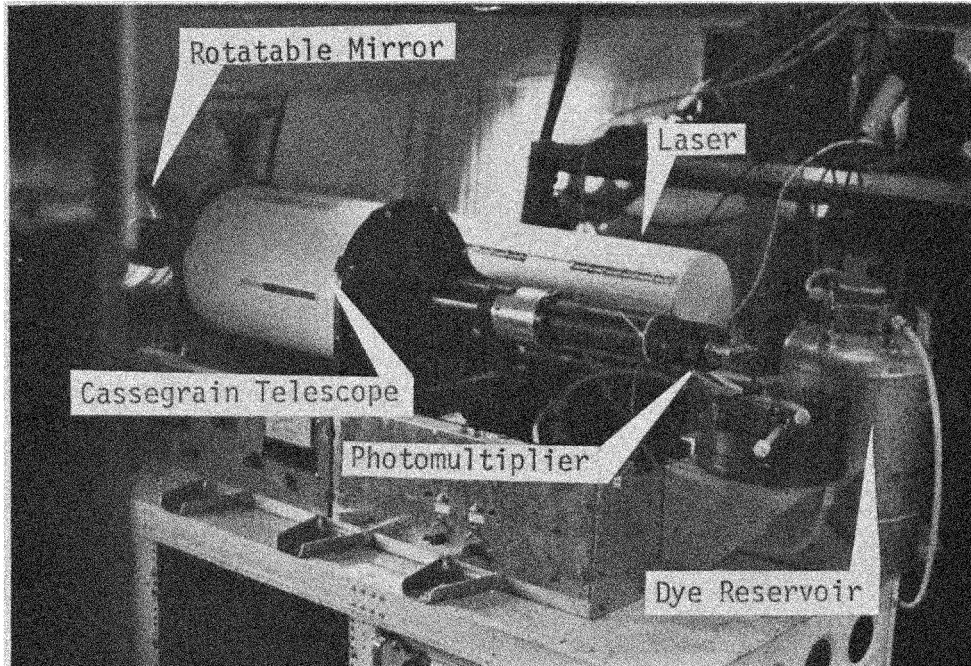


Fig. 14. Components of lidar system.



Fig. 15. Nephelometer display (upper left) and analyzing and recording electronics of lidar system.

background signal. The present nephelometer is a low-power instrument, taken very closely from a Venus lander design. Plans have been made to beef up the system for future aircraft use.

#### 2.4.9 Other Equipment

Some other user-oriented features of the Electra are listed below:

1. 16-mm time-lapse cameras are mounted on either side of the rear cabin, looking out the window to record cloud patterns during the flights. These are adjustable from zero to twenty frames per second. The present experiment used them at 1/4 to 1/5 frame per second.

2. The nose forward-looking radar may be viewed on any of the six TV monitors in the cabin.

3. A forward-looking TV camera is located in the cockpit. This may also be called up on the TV monitors.

4. The radar, the forward-looking TV, or the display of flight and meteorological parameters (section 2.4) may, at the discretion of the senior scientist, be recorded on videotape.

5. In addition to the strip chart mentioned previously, an electrostatic printer records flight data at seven second intervals. An example is shown in Fig. 17. Parameters included are time, aircraft latitude and longitude, wind direction and speed, vertical wind speed (in Fig. 17, this has been replaced by geometric altitude), pressure altitude, air temperature, dew point, potential temperature, sea surface temperature, and static pressure. The printer was also used on one or two flights to periodically output data from some of the radiation instrumentation.

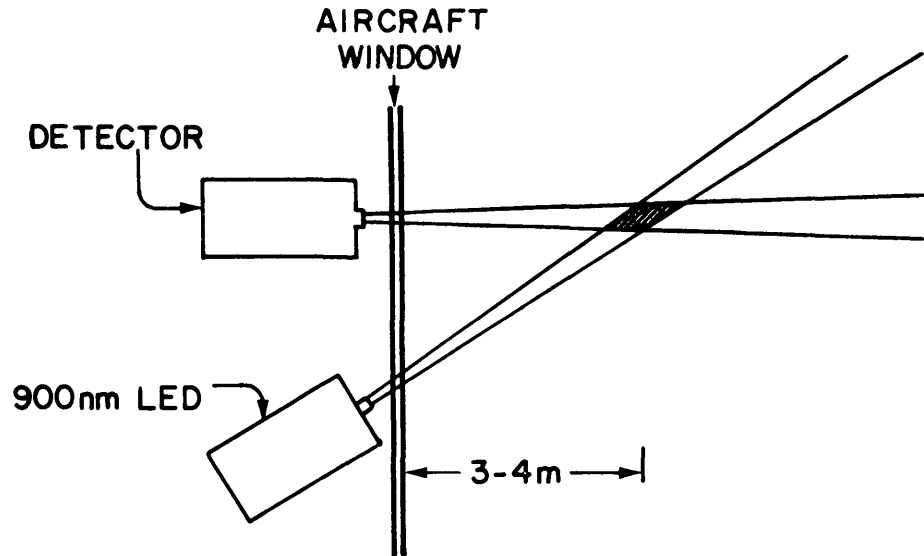


Fig. 16. Schematic diagram of nephelometer system.

TIME	LAT.	LONG.	WD/V	VWS	PALT	ATF	D. P.	THETA	RST	PRES
12: 7:19	37 71	-124.86	19/23	570	572	20.9	-0.7	299.2	10.0	941.1
12: 7:26	37 71	-124.86	20/25	542	544	20.0	1.4	298.0	11.1	944.3
12: 7:34	37 71	-124.87	19/24	513	513	19.4	3.1	297.1	10.6	947.7
12: 7:41	37 72	-124.87	19/24	481	481	19.4	3.2	296.8	10.4	951.4
12: 7:48	37 72	-124.87	15/26	447	448	17.6	5.7	294.6	10.8	955.1
12: 7:56	37 73	-124.88	2/24	415	413	11.9	8.7	288.5	11.1	959.2
12: 8: 3	37 73	-124.88	356/21	388	386	9.4	9.2	285.7	10.5	962.3
12: 8:10	37 73	-124.89	359/23	362	358	9.4	9.1	285.5	11.0	965.5
12: 8:18	37 74	-124.89	357/19	337	332	9.4	9.4	285.2	10.9	968.5
12: 8:25	37 74	-124.90	354/19	307	300	9.6	9.6	285.0	11.7	972.2
12: 8:32	37 75	-124.90	356/20	275	267	9.8	9.6	284.9	11.9	976.0
12: 8:40	37 75	-124.91	356/19	253	246	10.0	9.8	284.9	11.9	978.5
12: 8:47	37 75	-124.91	1/19	239	231	10.1	10.1	284.9	11.8	980.3
12: 8:54	37 76	-124.91	356/19	219	211	10.3	9.9	284.9	11.7	982.6
12: 9: 2	37 76	-124.93	354/18	204	195	10.5	10.2	284.9	11.8	984.5
12: 9: 9	37 77	-124.93	354/18	188	177	10.6	10.3	284.8	11.6	986.6
12: 9:16	37 77	-124.94	353/20	167	159	10.6	10.4	284.6	11.7	988.8
12: 9:24	37 79	-124.94	352/20	150	141	10.8	10.2	284.7	11.6	990.8
12: 9:31	37 79	-124.95	351/18	146	136	11.0	10.3	284.8	11.6	991.4
12: 9:38	37 79	-124.95	352/19	134	125	11.1	10.3	284.9	11.6	992.7
12: 9:46	37 80	-124.96	347/19	132	128	11.1	10.3	284.8	11.5	992.4
12: 9:53	37 80	-124.96	353/19	178	169	10.7	10.3	284.9	11.6	987.6
12:10: 0	37 80	-124.97	352/21	214	208	10.3	10.2	284.8	11.4	983.1
12:10: 8	37 80	-124.97	355/22	245	240	10.0	10.0	284.9	11.2	979.3
12:10:15	37 81	-124.98	352/20	270	264	9.8	9.9	284.9	11.2	976.5
12:10:22	37 81	-124.98	354/21	279	275	9.7	10.0	284.9	10.9	975.2
12:10:30	37 82	-124.99	357/23	286	281	9.7	9.6	284.9	11.1	974.4

Fig. 17. Sample of electrostatic printer output.

## 2.5 Base of Operations

Since satellite images were of great importance in planning the individual missions, we chose to base our operations in the San Francisco area, in order to have access to the National Environmental Satellite Service Office in Redwood City, California.

The field chosen was the Moffett Naval Air Station at Mountain View, California. We arranged to use NASA's (Ames Research Center) hangar and ramp facilities.

The Satellite Service was able to supply us with GOES visible images every hour during daylight and infrared images hourly throughout the day. We were also able to obtain a NOAA-3 or NOAA-4 image once each day. Some of the GOES images are included in section 3.

### 3.0 FIELD PHASE OF THE MARINE STRATOCUMULUS EXPERIMENT

The Marine Stratocumulus Experiment was carried out between 01 June and 18 June 1976. Section 3.1 gives a description of each of the five flights, and section 3.2 describes some related measurements taken during the field phase.

#### 3.1 The Research Flights

Five research flights were carried out during this experiment. Table V summarizes the flight operations. For each flight the following information is presented:

1. A brief description of the flight.
2. A map of the flight pattern. (The discrepancies between the initial and final coordinates are caused by INS errors.)
3. A visible satellite image. Images were chosen as near to the middle of the flight period as possible (visible images were not available until 1415 Z, and not of good quality over the eastern Pacific until 1515 Z or 1615 Z).
4. One or two soundings. Data were taken from the electrostatic printer records. Times were chosen on the basis of the depth of the sounding in order that the inversion be sufficiently covered. Winds are in  $\text{ms}^{-1}$  with a full barb representing  $5 \text{ ms}^{-1}$  and a half-barb  $2.5 \text{ ms}^{-1}$ .

TABLE V. SUMMARY OF FLIGHTS

DATE 1976	05 June	07 June	12 June	13 June	17 June
Takeoff (Z)	1818	1804	1144	1159	1130
Landing (Z)	2344	2227	1841	1922	1633
Duration	5 h 26 min	4 h 23 min	6 h 57 min	7 h 23 min	5 h 03 min
Total # of Flight Legs/ # of Locations	10/2	6/1	21/5	16/3	12/2
Equipment Problems	no lidar, noisy radi- ation data	no lidar broken wet bulb thermistor	no lidar	no lidar	no lidar, no FSSP data

Flight #1: 05 June 1976

The first flight went the farthest south of the five. Takeoff was at 1818 Z (1118 PDT). The stratocumulus deck was very thin, averaging 200 m or less in thickness. Two sets of legs were flown. The first five legs were at altitudes of 60 m, 425 m, 850 m, 900 m, and 1050 m. The second set of five legs were at altitudes of 60 m, 425 m, 800 m, 900 m, and 850 m. In between the two sets of legs soundings were made from 900 hPa to 1016 hPa and back to 900 hPa.

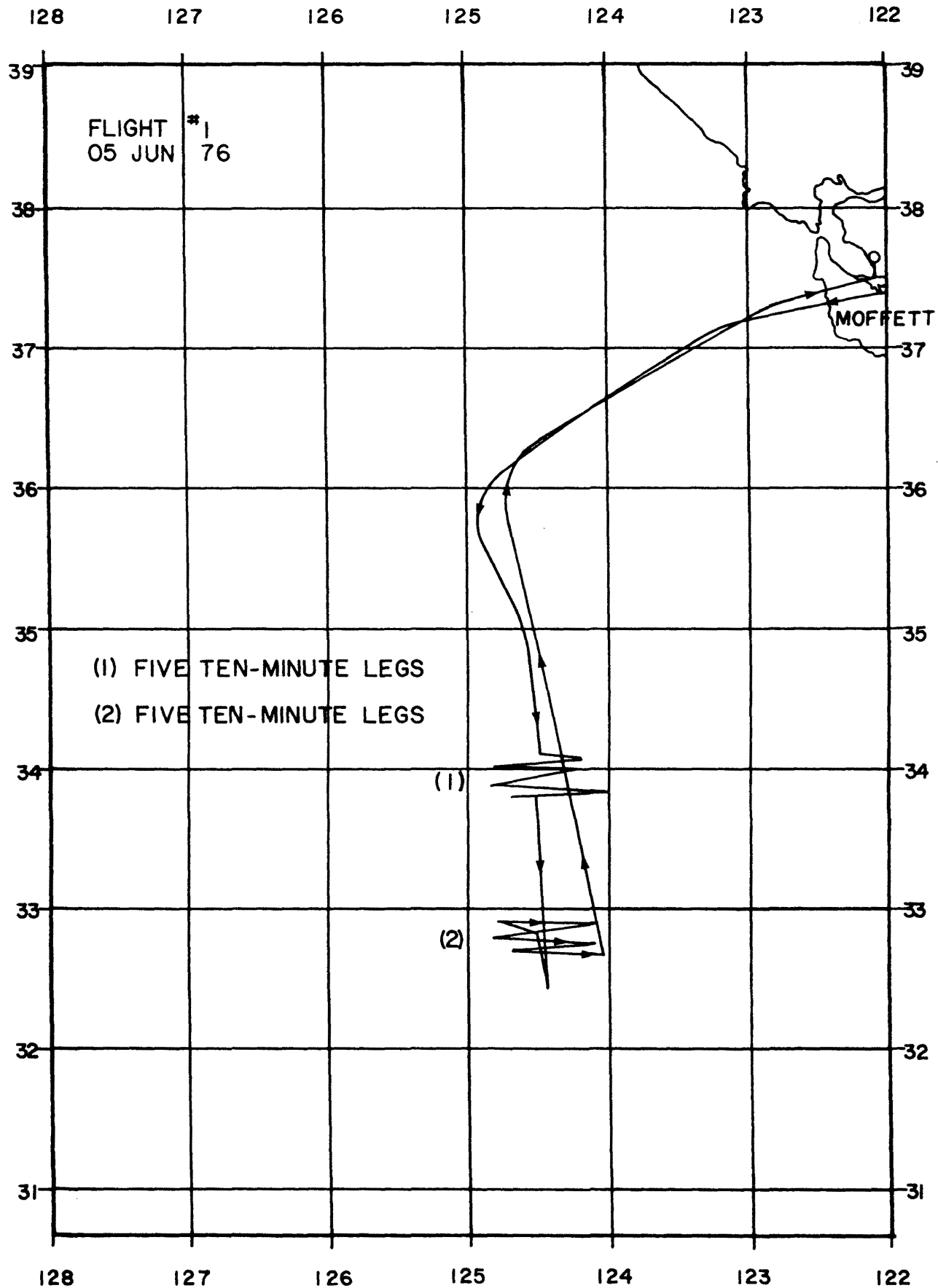


Fig. 18. Aircraft track for flight #1, 5 June 1976.

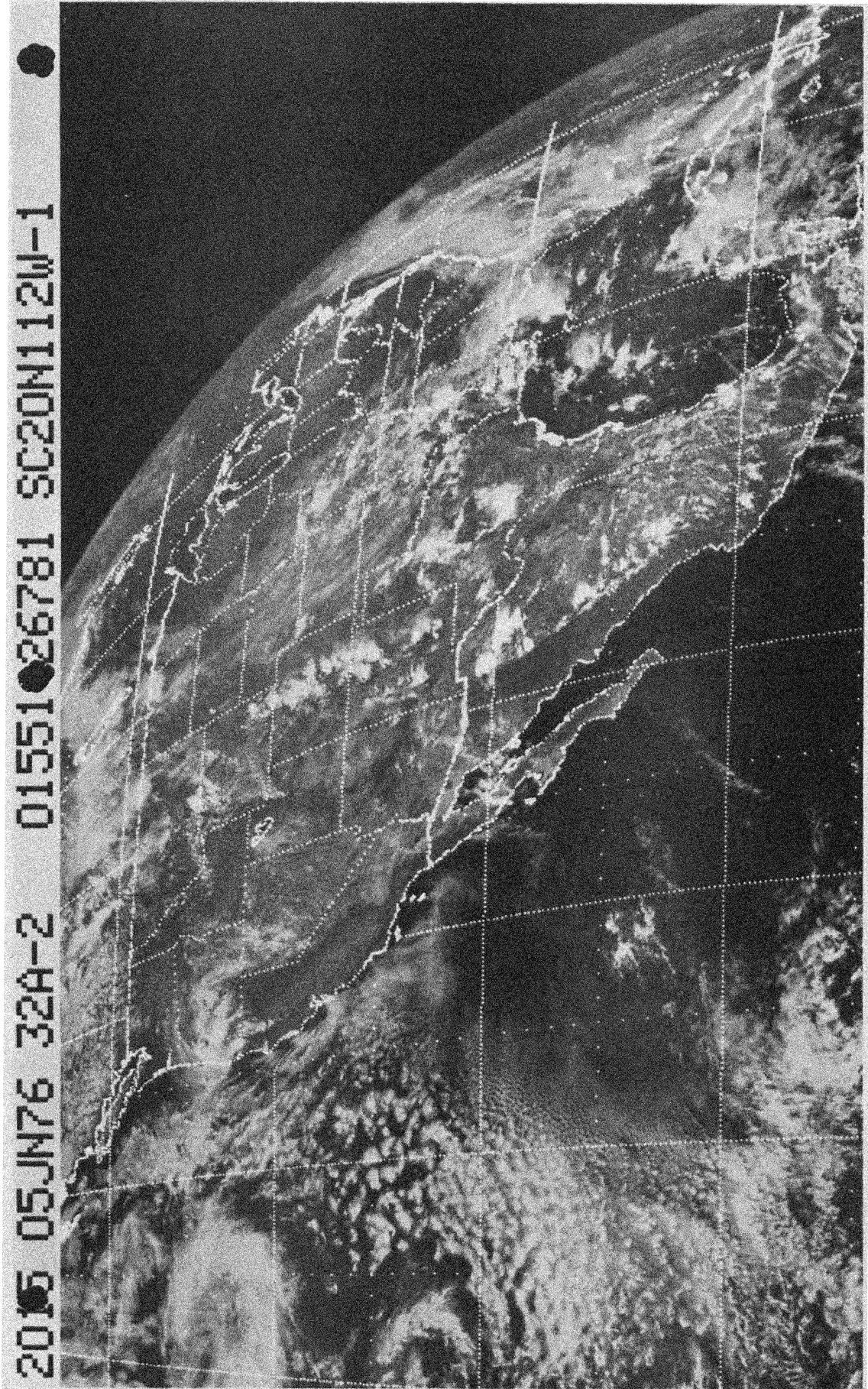


Fig. 19. SMS/GOES visible image for 2015 Z, 5 June 1976.

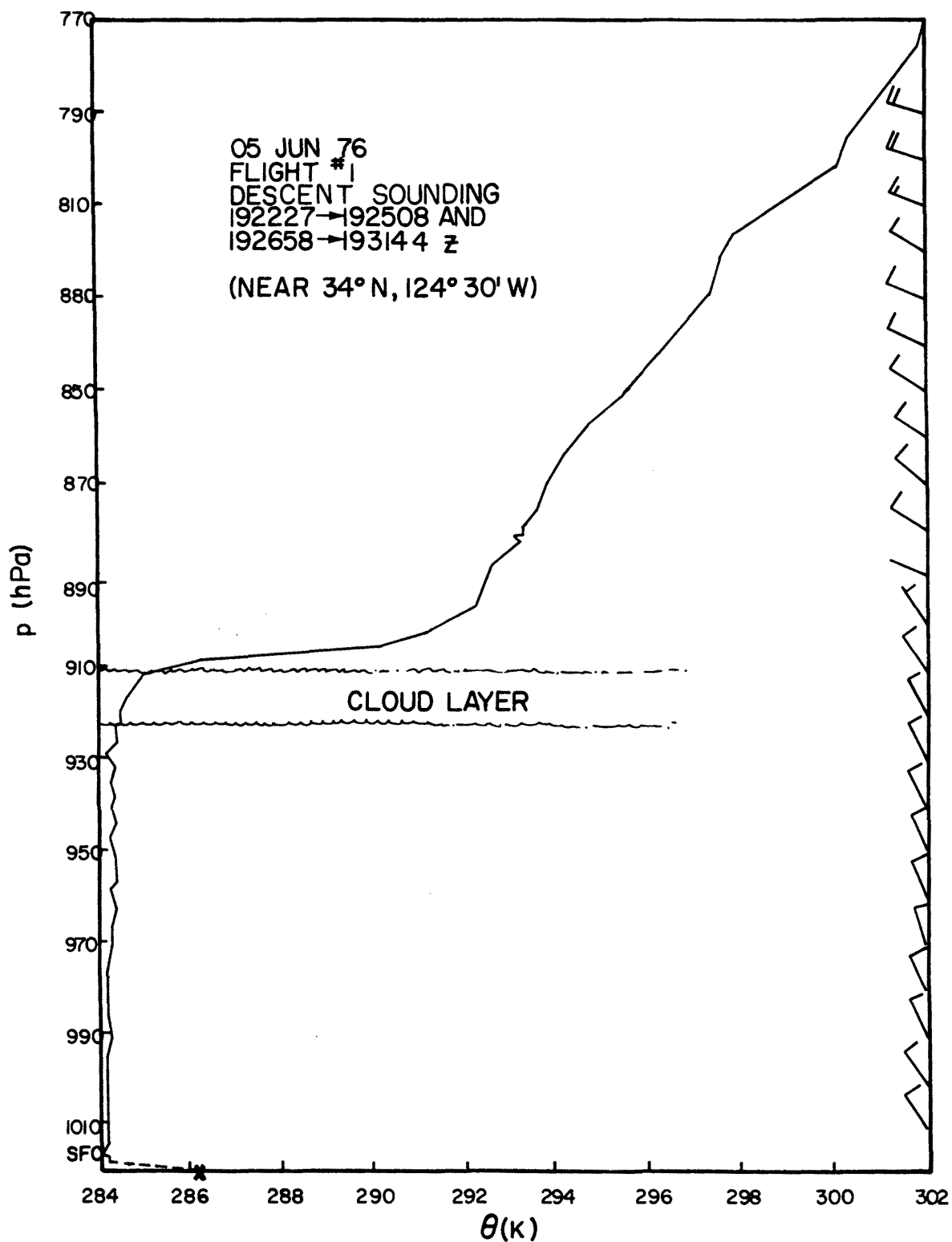


Fig. 20. Potential temperature and wind profiles obtained during descent to site (1) in Fig. 18.

Flight #2: 07 June 1976

Conditions in the flight area on this date were very confused, consisting of a stratocumulus deck interspersed with shallow but active convective clouds. The situation being contrary to the sort of conditions in which we were interested, the flight was aborted after one set of six legs, which were flown at altitudes of 60 m, 450 m, 900 m, 1350 m, 1800 m, and 2700 m. The stratocumulus deck was very high, with cloud base at about 1200 m and cloud top above 2000 m. Some precipitation was encountered, resulting in the breakage of the wet bulb thermistor. The cloud top appeared to rise during the flight. This case is of interest because it represents the breakdown of the classical stratocumulus deck during the passage of an upper level trough.

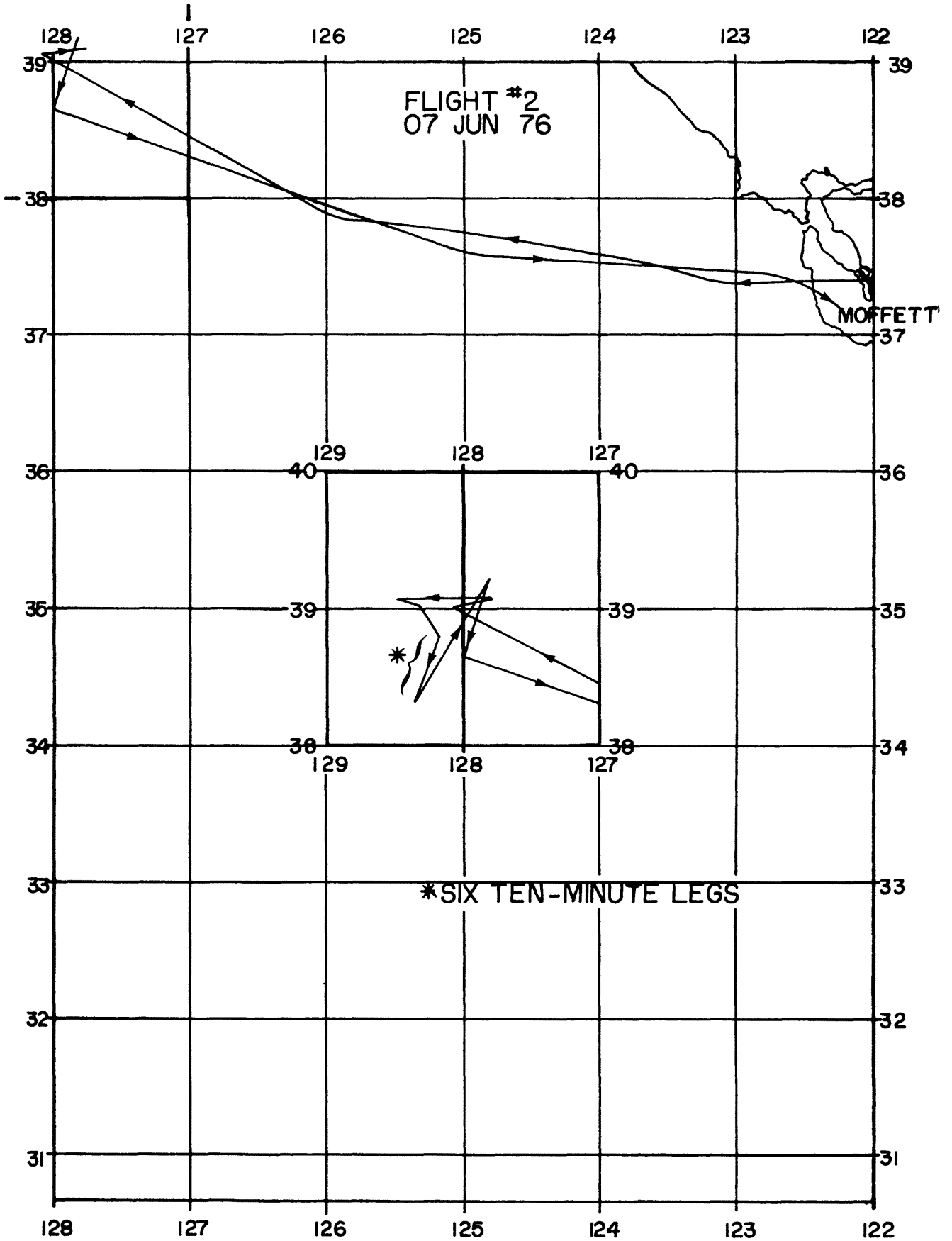


Fig. 21. Aircraft track for flight #2, 7 June 1976.

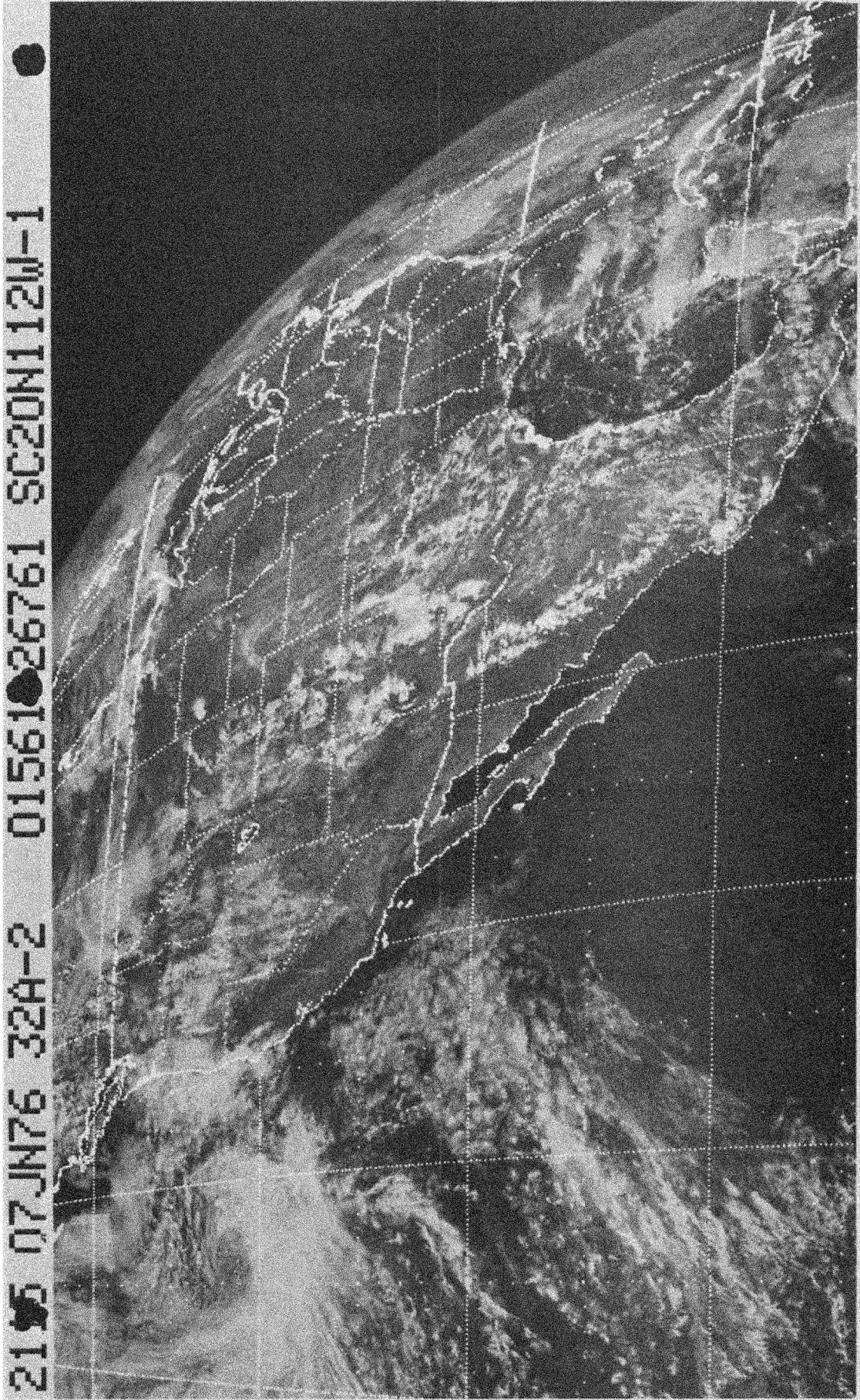


Fig. 22. SMS/GOES visible image for 2115 Z, 7 June 1976.

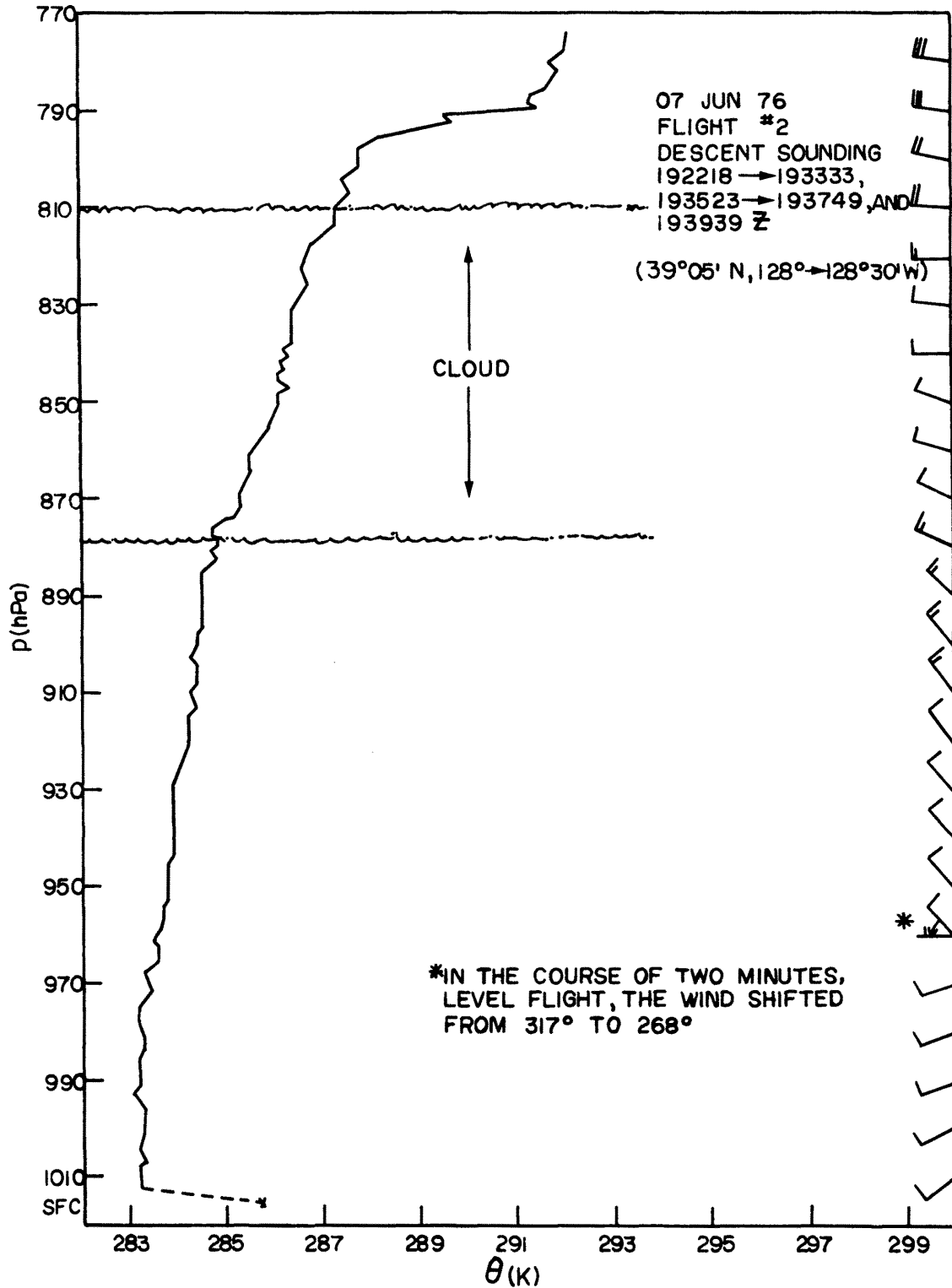


Fig. 23. Potential temperature and wind profiles obtained during initial descent of flight #2.

Flight #3: 12 June 1976

On 12 June an extensive stratocumulus deck covered the area off the northern California coast. A total of twenty-one turbulence legs were flown at five locations. Wind speeds as high as  $20 \text{ ms}^{-1}$  at 600 m MSL were observed. Cloud tops were in the range of 700 m to 900 m, with cloud base below 40 m on occasion. The first set of legs, on the east side of the box, were at 730 m, 275 m, 215 m, 125 m, and 520 m. On the north side of the pattern, legs were flown at 90 m, 760 m, 370 m, 250 m, and 150 m. The legs on the west side were flown crosswind, as can be seen in Fig. 24 (winds were generally from about  $350^\circ$ , see Figs. 26 and 27). The legs were at altitudes of 670 m, 450 m, 250 m, and 60 m. The fourth set, at the south, were at 730 m, 550 m, 300 m, and 60 m. The final set were in the same area as the first set, but six hours later (1800 to 1830 Z) and were flown at 120 m, 275 m, and 730 m.

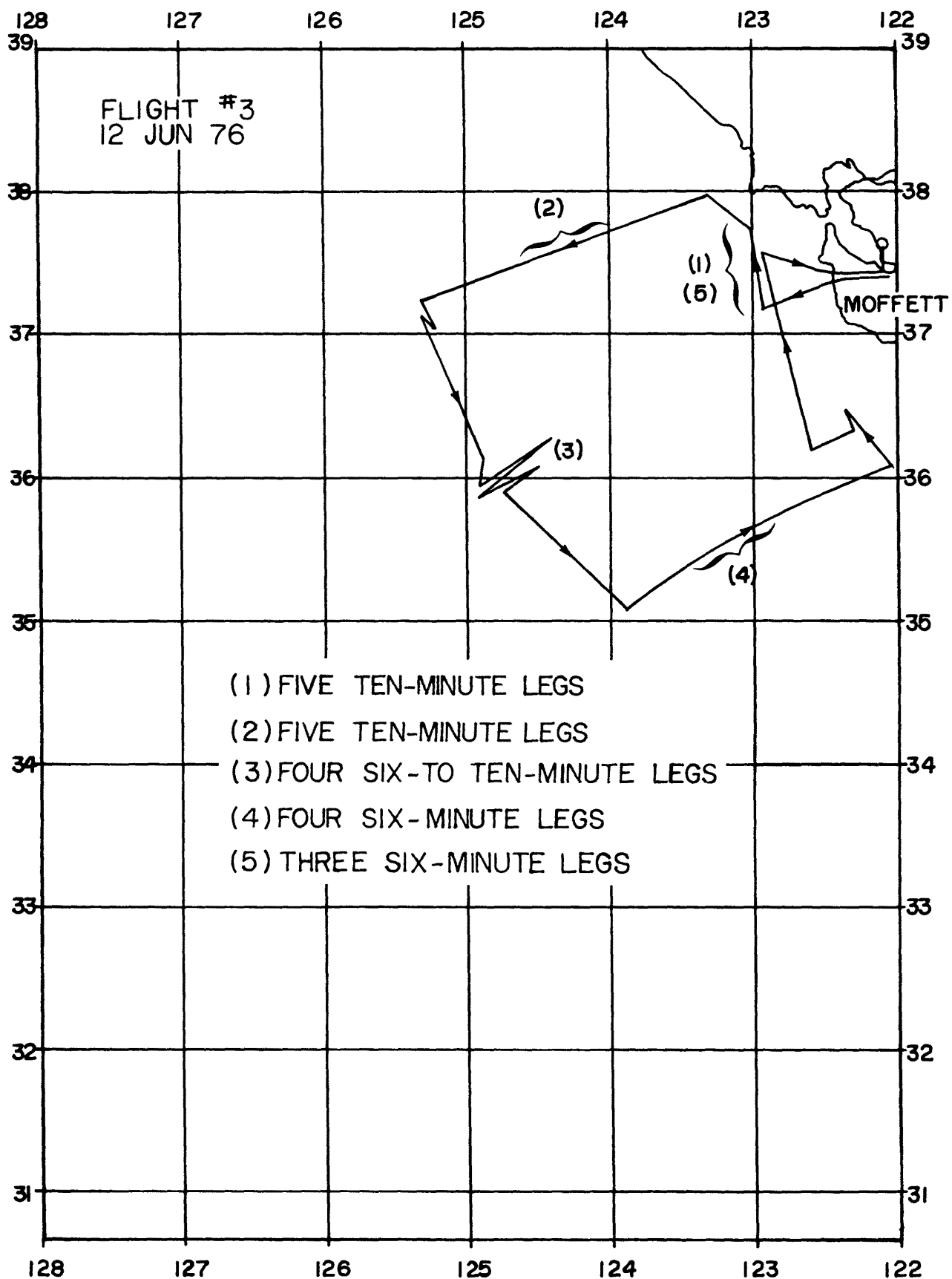


Fig. 24. Aircraft track for flight #3, 12 June 1976.

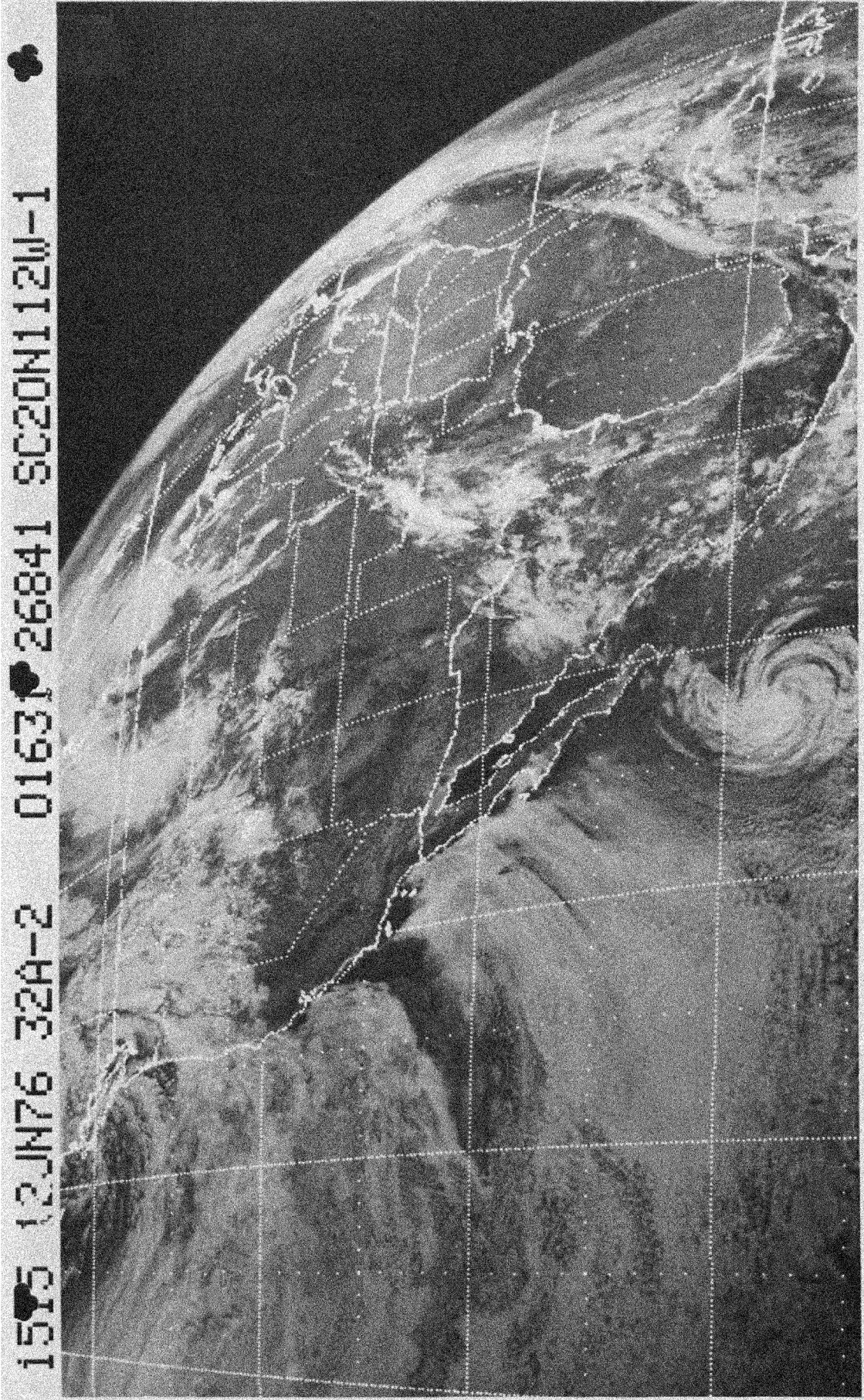


Fig. 25. SMS/GOES visible image for 1515 Z, 12 June 1976.

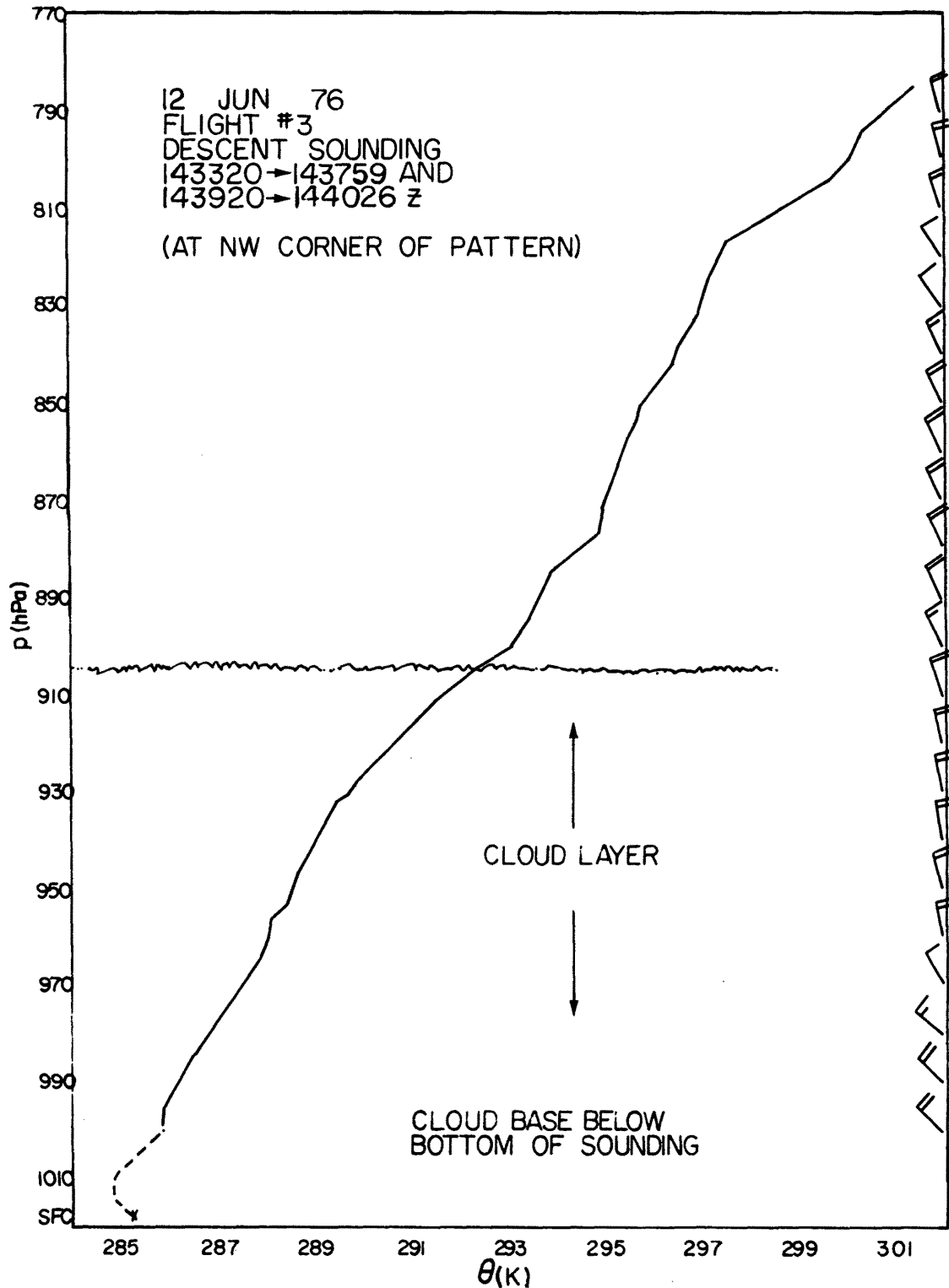


Fig. 26. Potential temperature and wind profiles obtained at the north-west corner of flight pattern shown in Fig. 24.

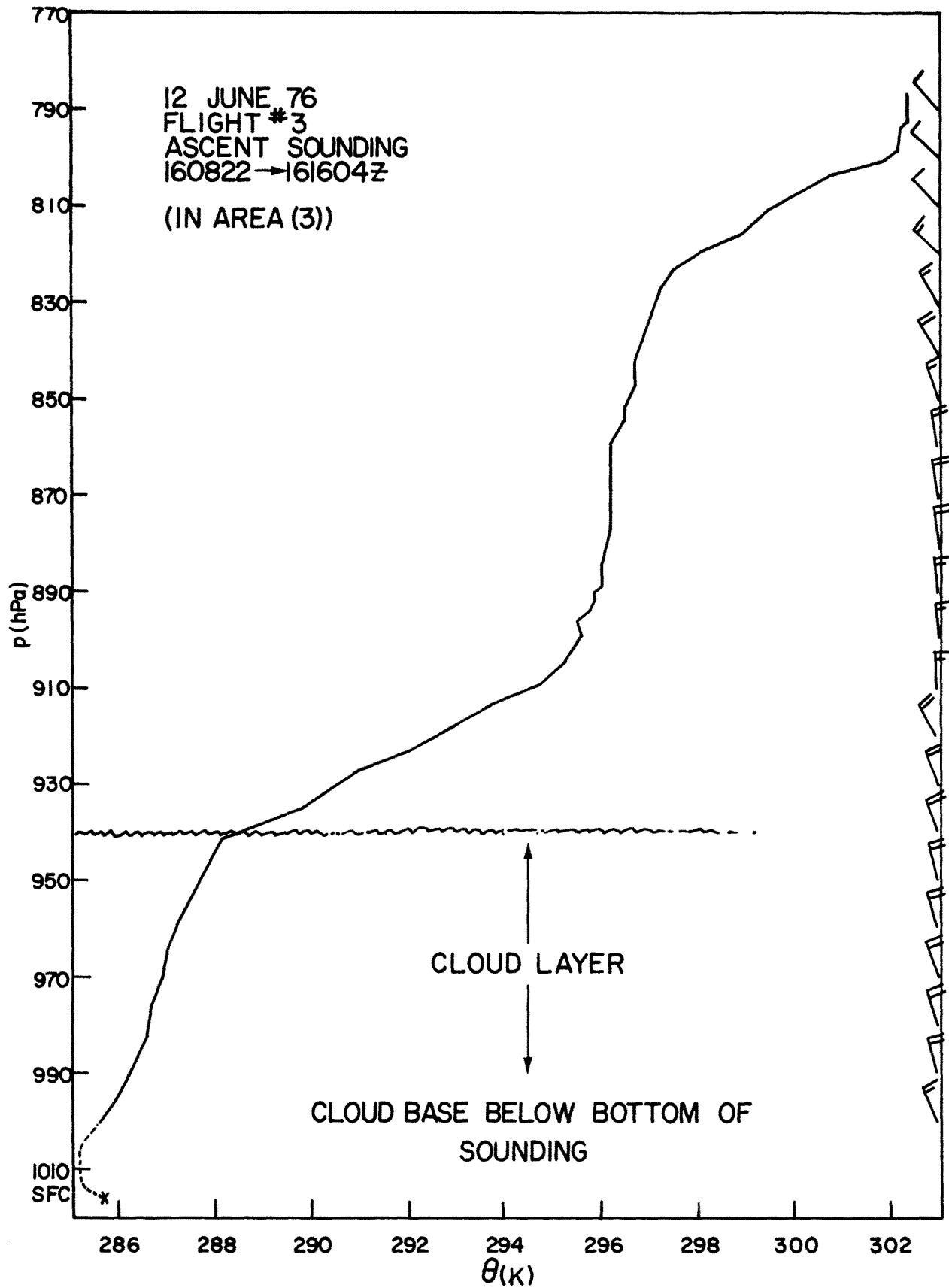


Fig. 27. Potential temperature and wind profiles obtained on the western side of flight pattern shown in Fig. 24.

Flight #4: 13 June 1976

Our longest flight was the fourth one, a total of 7 hours and 23 minutes between take-off and touch-down. Sixteen ten-minute legs were flown in three locations. The first set were on the south side of the box, at altitudes of 60 m, 180 m, 275 m, 365 m, and 600 m. The second and third sets were to the north, with the second set at the same heights as the first and to the east of the third set, which were also at the same height, except for the addition of a leg at 490 m.

Before the first set of legs soundings were flown on the east side of the box from 60 m to 600 m and back  $2\frac{1}{2}$  times (ending at 600 m). In between the first and second sets, a similar pattern was flown between 60 m and 1370 m, and again between the second and third sets.

At the eastern edge of the pattern the clouds were very thin (about 100 m in thickness) and the inversion was not very pronounced, while clouds toward the west were thicker, and the inversion was stronger. This point is illustrated by comparison of the two soundings presented in Figs. 30 and 31.

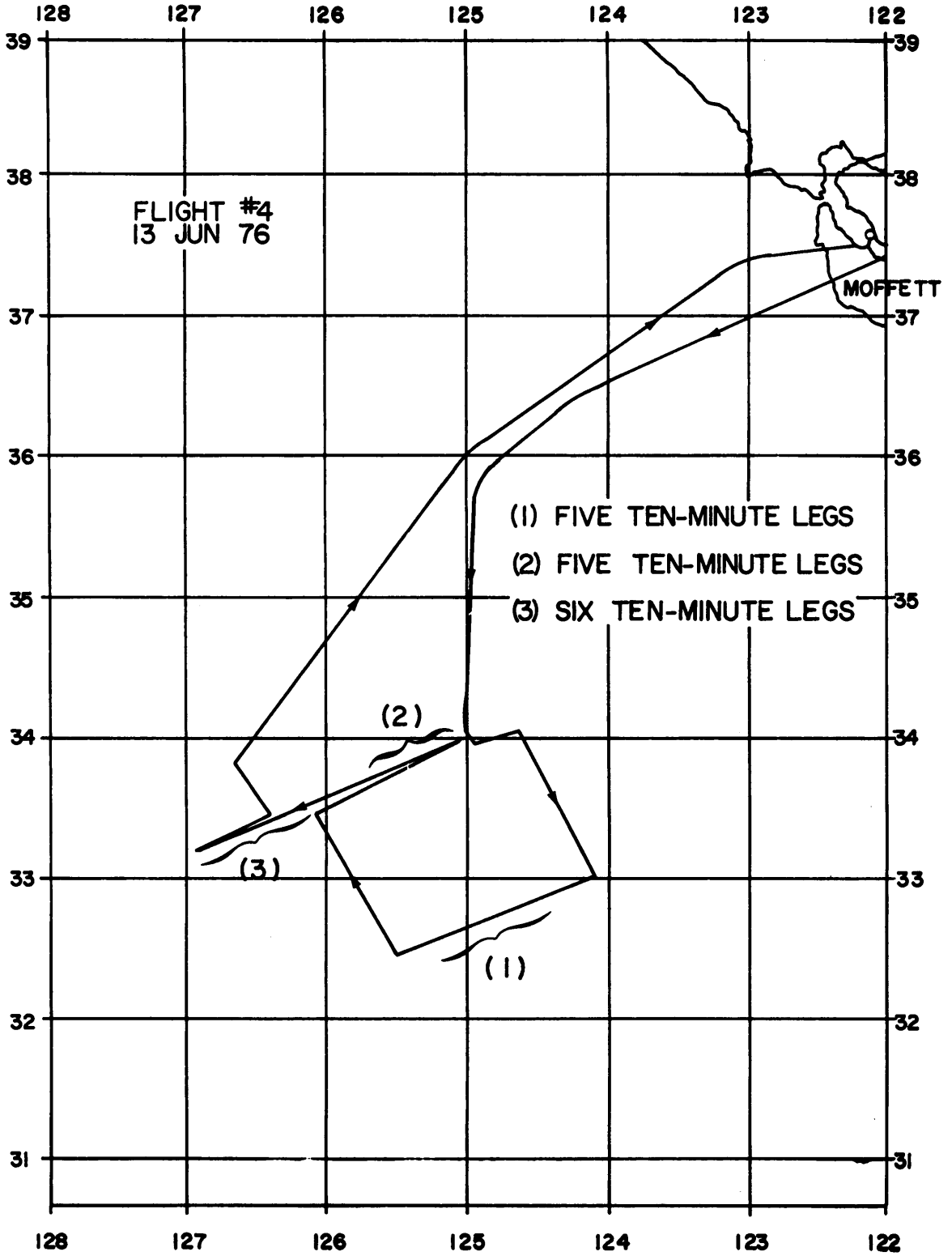


Fig. 28. Aircraft track for flight #4, 13 June 1976.

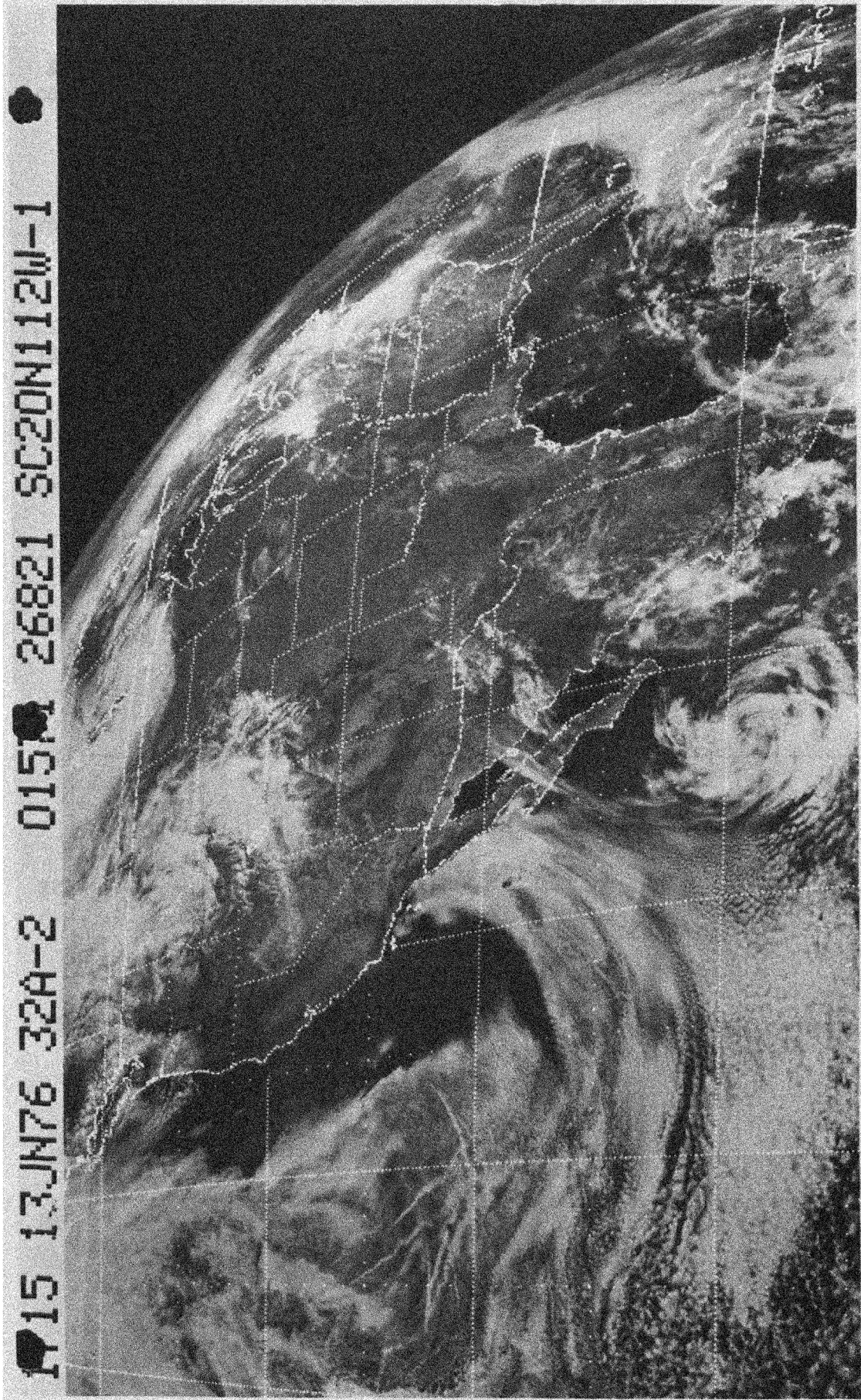


Fig. 29. SMS/GOES visible image for 1715 Z, 13 June 1976.

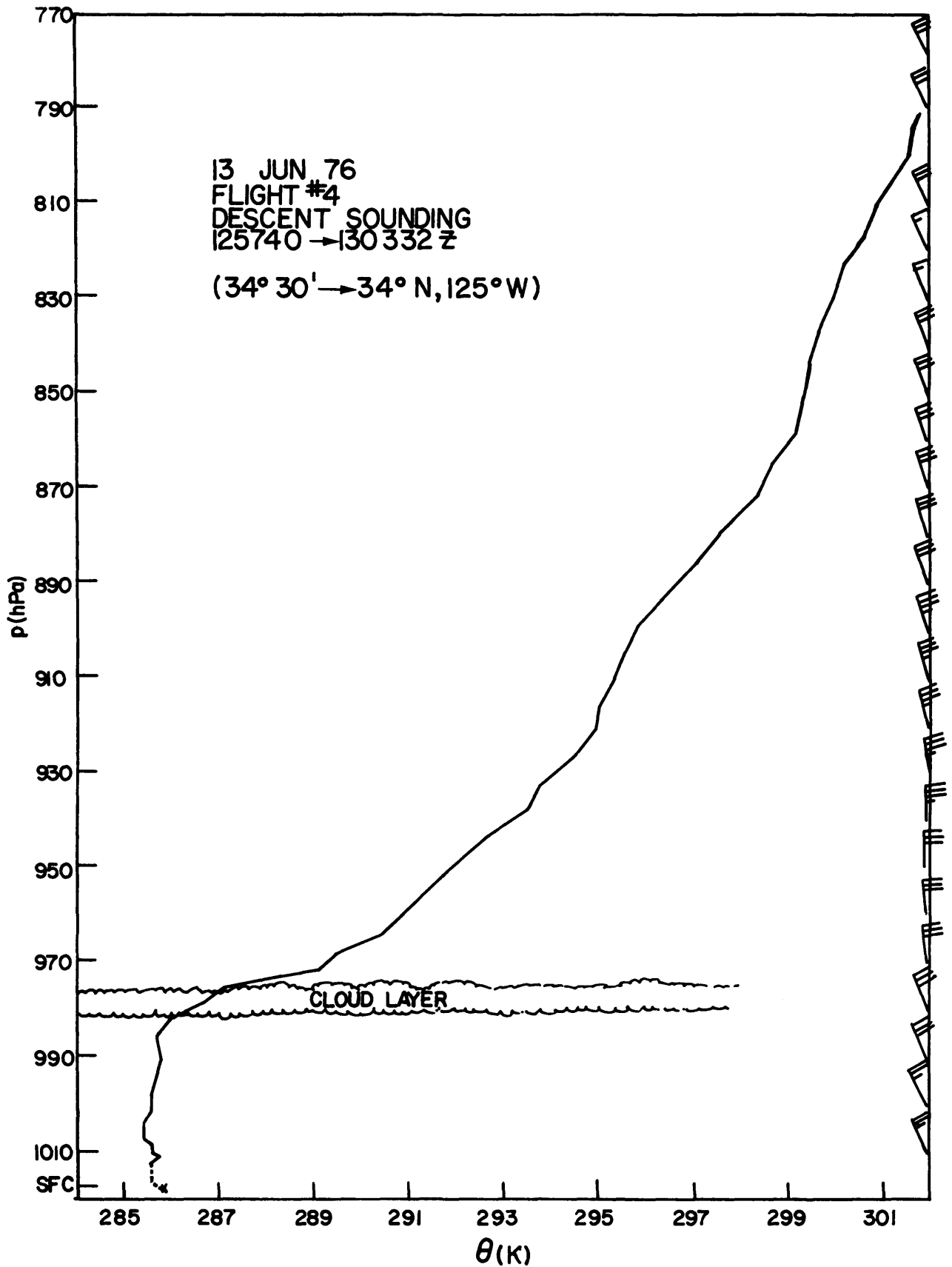


Fig. 30. Potential temperature and wind profiles obtained during initial descent of flight #4.

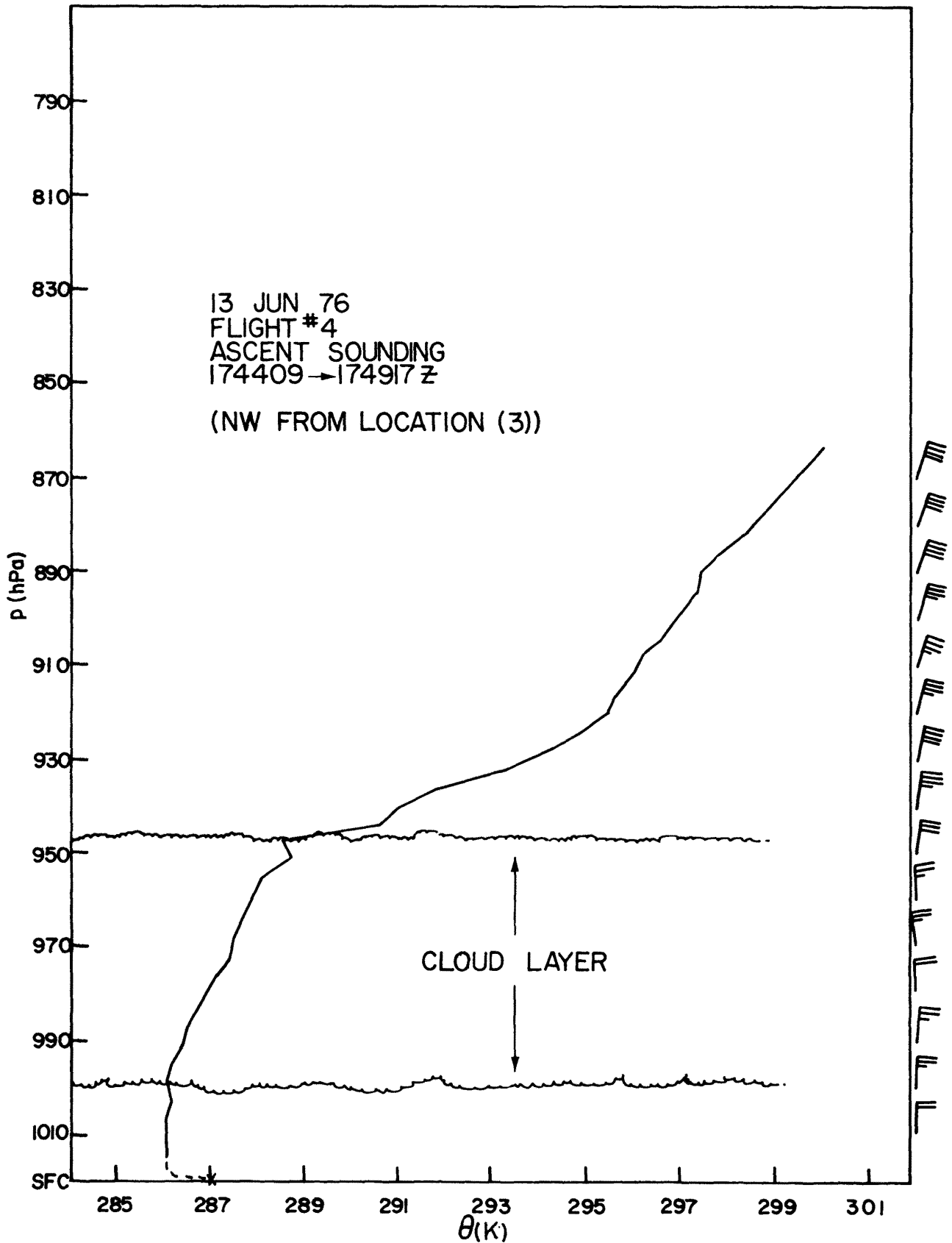


Fig. 31. Potential temperature and wind profiles obtained just north-west of location (3) in Fig. 28.

Flight #5: 17 June 1976

Our last flight was extremely interesting with a very strong inversion capping the clouds, as shown in Fig. 34. A total of twelve ten-minute turbulence legs were flown, at two locations, with soundings between. The cloud deck was fairly thin, lying between about 200 m and 450 m MSL. The first set of legs were flown at altitudes of 760 m, 430 m, 300 m, 180 m, and 60 m, while the second set were at 60 m, 170 m, 275 m, 380 m, 490 m, 600 m, and 700 m.

The sounding shows the structure of the cloud and inversion layers quite well. A moist adiabat is followed through the cloud, and a strong inversion of about  $11^{\circ}\text{C}$  in 10 hPa is found just above cloud top. Surprisingly strong winds, greater than  $20\text{ ms}^{-1}$  in the mixed layer, were observed on the flight.

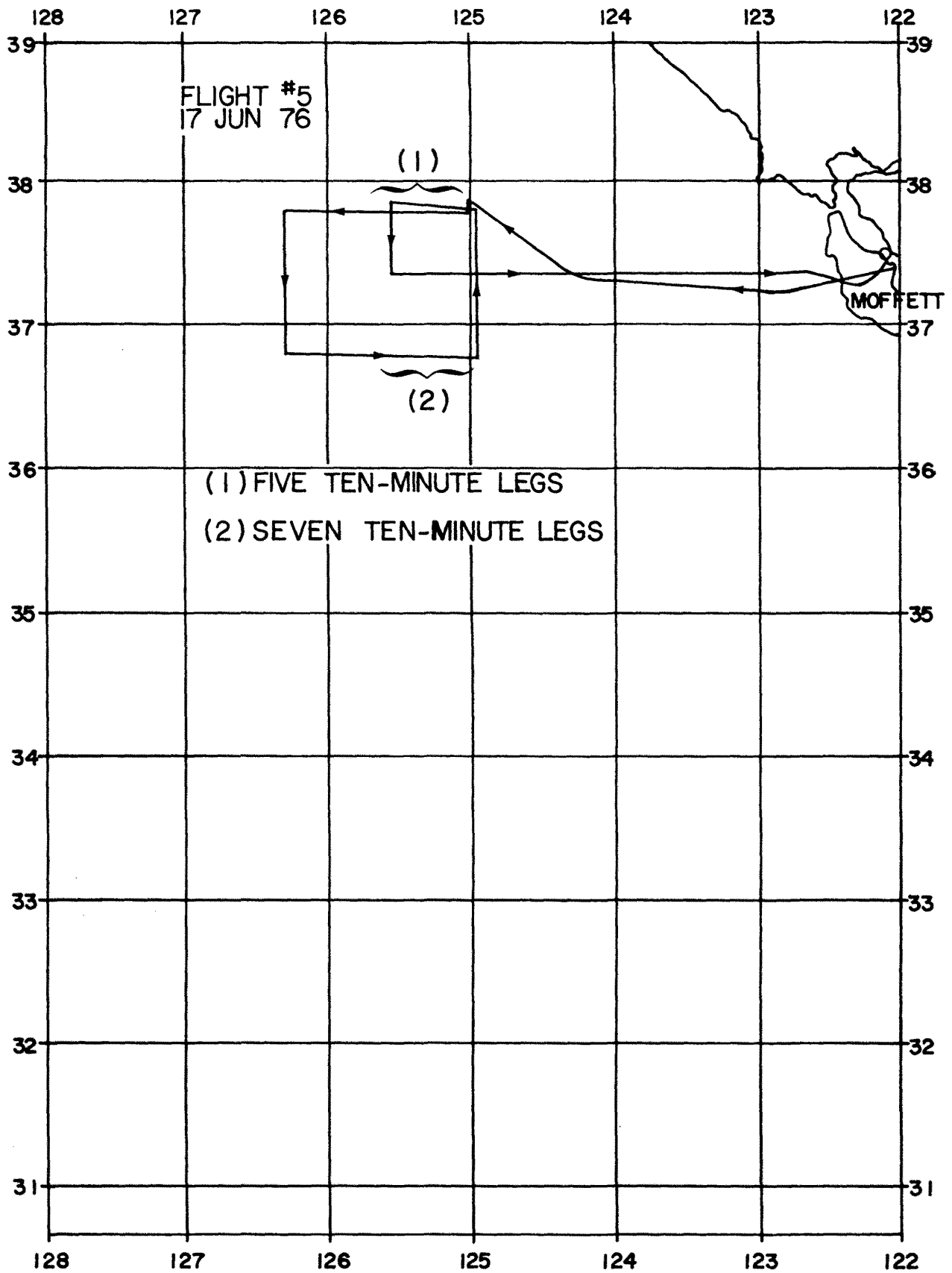


Fig. 32. Aircraft track for flight #5, 17 June 1976.



Fig. 33 SMS/GOES visible image for 1615 Z, 17 June 1976.

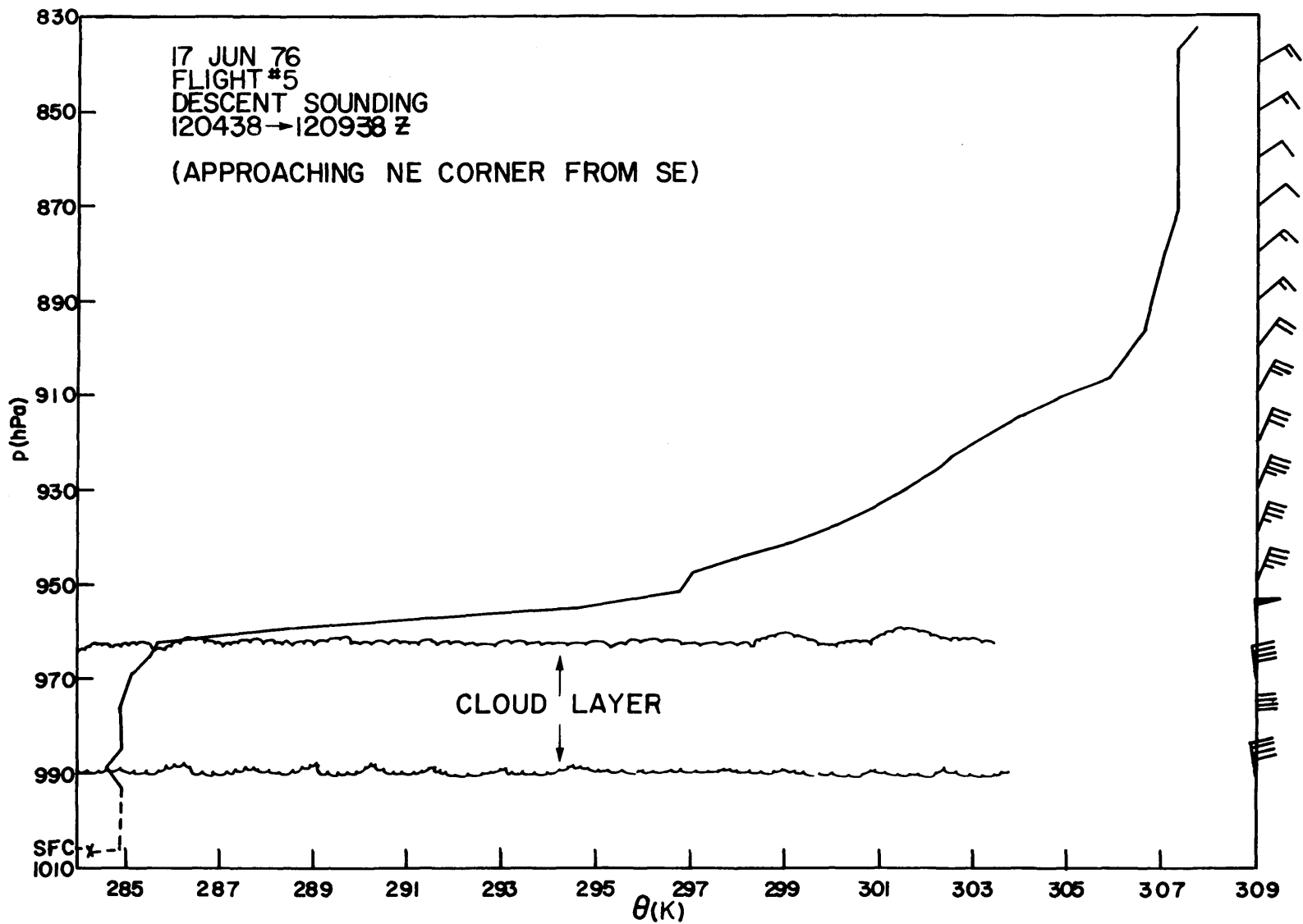


Fig. 34. Potential temperature and wind profiles obtained during initial descent to northeast corner of box pattern shown in Fig. 32.

### 3.2 Related Measurements

#### BOUNDARY LAYER STUDIES

Boundary layer studies in the San Francisco area are currently being carried out by a group from San Jose State University (Goodman, 1975; Miller, 1975, 1976). The group, led by Albert Miller, has instrumented the Mt. Sutro television tower in San Francisco (see Figs. 35, 36, and 37) at twelve levels. The tower rises from the top of 250 m high Mt. Sutro to a height of 470 m MSL, often extending through the coastal marine layer into the inversion layer above. Measurements taken include temperature and dew point, pressure, three components of wind, radiation, liquid water content, cloud droplet size distribution, cloud condensation nuclei concentration, and ozone concentration.

An attempt was made to coordinate our aircraft measurements with Miller's tower measurements. Although air traffic control regulations precluded any sort of "tower fly-by" with such a large aircraft, inter-comparisons between the two sets of data (especially for flight #3 and, to a lesser extent, #5) should be of value.

#### SATELLITE IMAGES

A group from Colorado State University, headed by T. H. Vonder Haar, is performing cloud analyses with GOES satellite images, using digital data collected at White Sands, New Mexico. During the operational period of the stratocumulus experiment, Vonder Haar's group shifted their HIPLEX grid far enough to the west to allow digital data coverage of our research area. This will allow correlation of high resolution digital satellite data with detailed aircraft soundings.

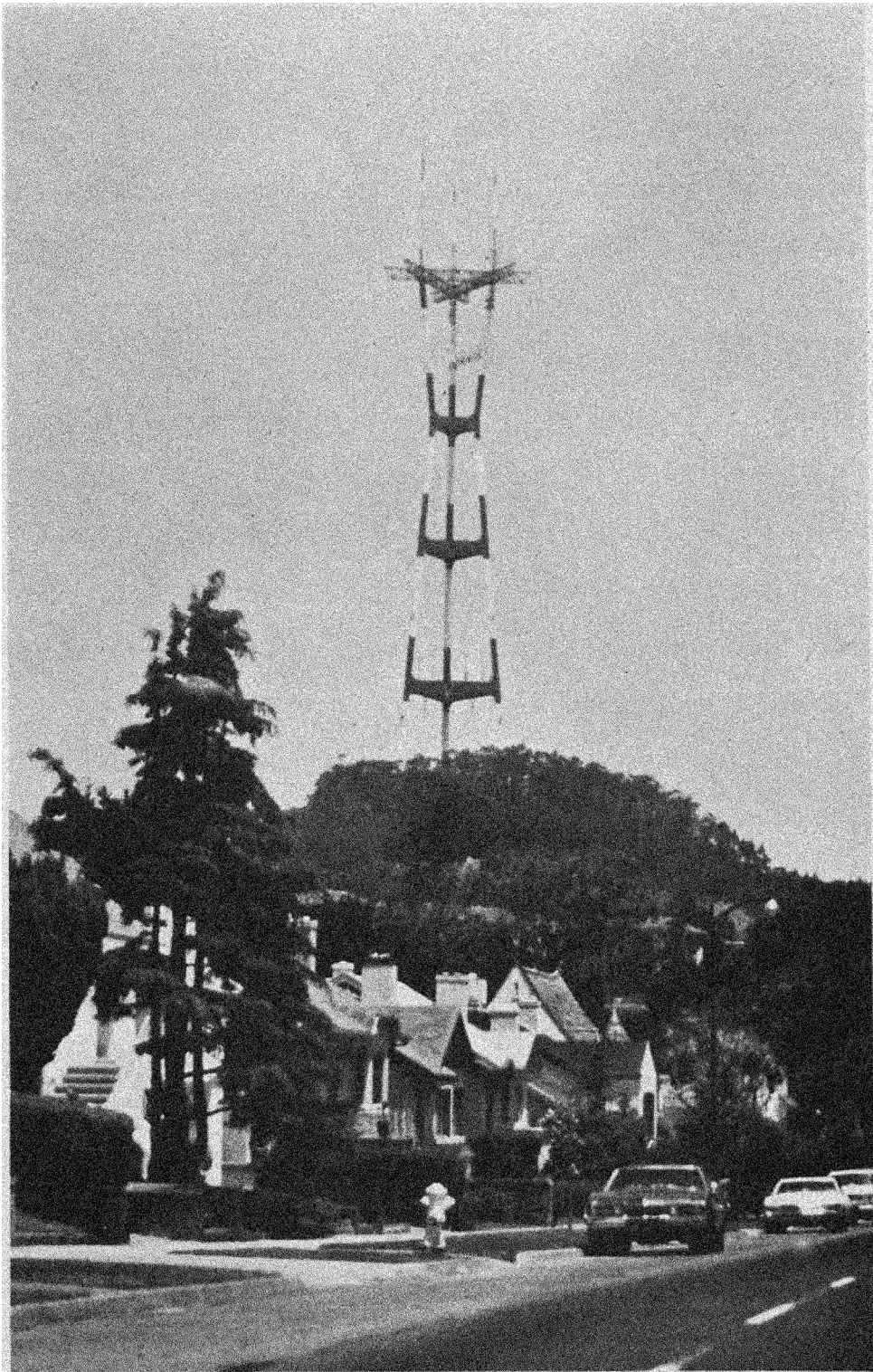


Fig. 35. Mt. Sutro television tower instrumented by San Jose State University.

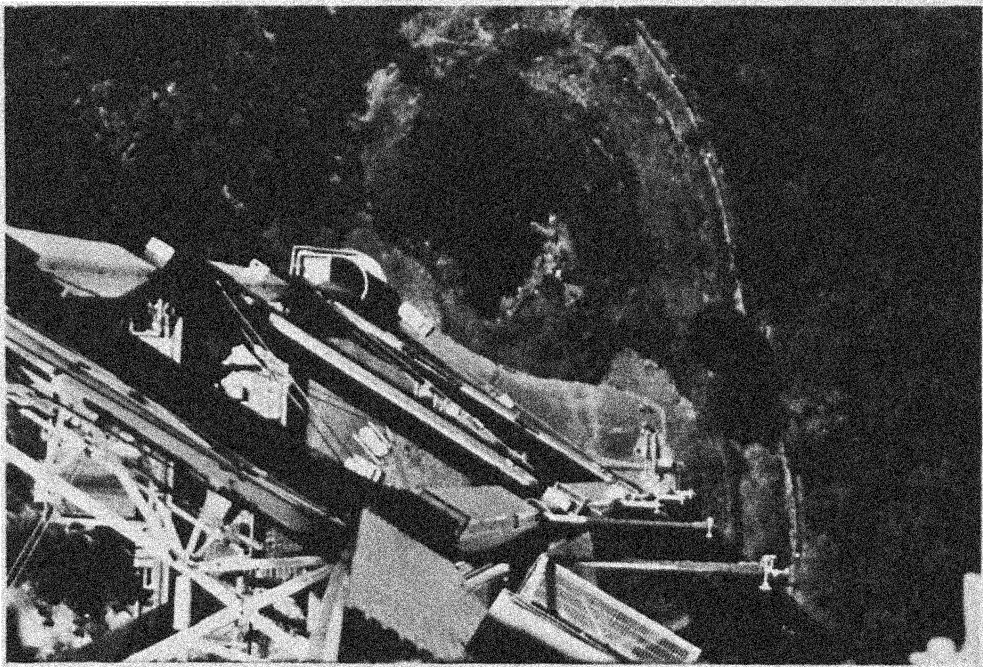


Fig. 36. View (looking down) of instrument booms.

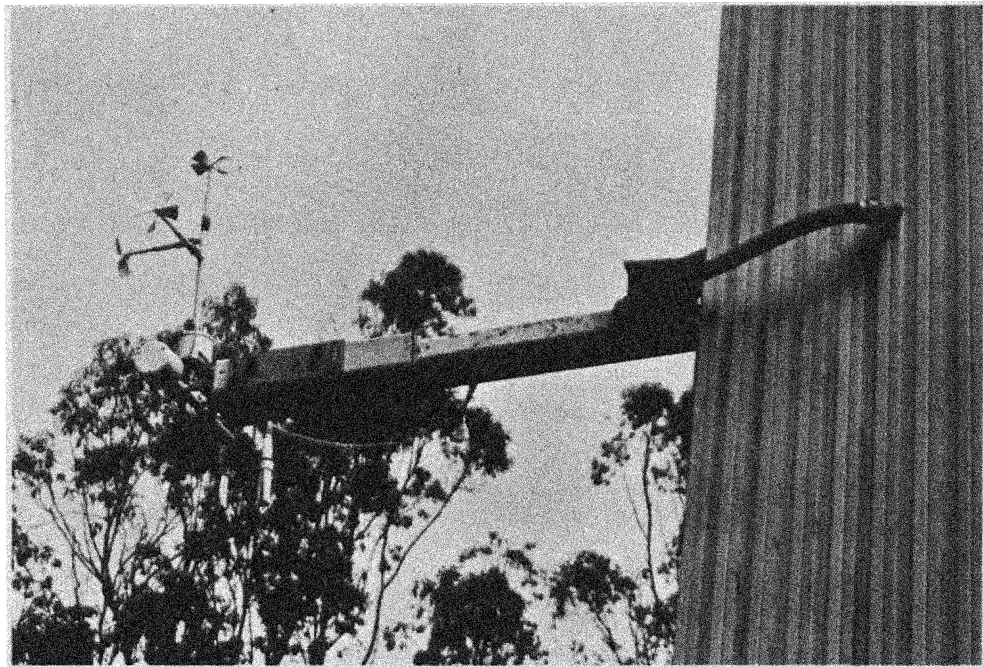


Fig. 37. Close-up of a Mt. Sutro tower instrument boom.

#### 4.0 CONCLUSIONS

Since it was so well equipped the Electra aircraft was apparently able to make all the necessary measurements set forth in Chapter 2, with the possible exception of 100-500 km scale wind observations of sufficient accuracy to allow computation of the large-scale horizontal divergence and vertical velocity. Such observations could perhaps best be obtained with an array of at least three ships equipped with tethered balloons. A program which included two aircraft and four ships would provide field flexibility in the event of equipment failures. Should ships be available for such a program, it would appear logical to expand the observational objectives to include the structure of the mixed layer of the upper ocean. Considerable interest presently exists in oceanic mixed layer modeling (e.g. Kraus and Turner, 1967; Denman, 1973; Denman and Miyake, 1973; Pollard et al., 1973; Gill and Turner, 1974; Niiler, 1975; Alexander and Kim, 1976; Kim, 1976). A combined atmospheric/oceanic observational program would stimulate the development of coupled atmospheric mixed layer/oceanographic mixed layer models for use in climate research. Such an effort is presently being planned as a GARP subprogram by radiation and convection researchers from several countries.

## ACKNOWLEDGEMENTS

We would like to express our sincere thanks to all the individual participants of the Marine Stratocumulus Project and to the NCAR Research Aviation Facility and Computing Facility. We are also indebted to Dorothy Chapman for her help in preparing this report.

The research described herein was supported by the National Science Foundation both through the National Center for Atmospheric Research and through Colorado State University, the latter under grants ATM 76-09370, OCD 74-21678, and by the National Aeronautics and Space Administration through grant GA 31588.

## REFERENCES

- Abbott, C. E., J. E. Dye, and J. D. Sartor, 1972: An electrostatic cloud droplet probe. J. Appl. Meteor., 11, 1092-1100.
- Albrecht, B. A., M. Poellot, and S. K. Cox, 1974: Pyrgeometer Measurements from aircraft. Rev. Sci. Instrum., 45, 33-38.
- \_\_\_\_\_, and S. K. Cox, 1976: Radiation Data Reduction Procedures for Sabreliner, C-130, and DC-6 Aircraft During the GARP Atlantic Tropical Experiment. CSU-ATSP-244, Department of Atmospheric Science, Colorado State University, 100 pp.
- Alexander, R. C., and J.-W. Kim, 1976: Diagnostic model study of mixed layer depths in the Summer North Pacific. J. Phys. Oceanogr., 6, 293-298.
- Arakawa, A., A. Mintz, et al., 1974: The UCLA Atmospheric General Circulation Model. Department of Meteorology, UCLA (available from the authors at the Department of Meteorology, University of California, Los Angeles 90024).
- Axford, D. N., 1968: On the accuracy of wind measurements using an inertial platform in an aircraft. J. Appl. Meteor., 7, 645-666.
- Ball, F. K., 1960: Control of inversion height by surface heating. Quart. J. Roy. Meteor. Soc., 86, 483-494.
- Barnes Engineering Company, 1971: Instruction Manual for Precision Filter Radiometer Model PRT-6, BEC16508607TM71, Barnes Engineering Company, 54 pp.
- Buck, A. L., 1975: Error sensitivity of fixed- and variable-path Lyman-alpha hygrometers. NCAR TN/EDD-103, National Center for Atmospheric Research, 45 pp.
- Burris, R. H., 1975: Flight Operations Instructions No. 7. National Center for Atmospheric Research, Atmospheric Technology Division, Research Aviation Facility, 2 pp.
- Deardorff, J. W., 1976: On the entrainment rate of a stratocumulus-topped mixed layer under a strong inversion. Quart. J. Roy. Meteor. Soc., (in press).
- DeLeo, R. V., and F. D. Werner, 1960: Temperature sensing from aircraft with immersion sensors. Instrument Society of America Proceedings, 1960 Conf., Vol. 15, Part 2, NY60-91, 1-10.

- Denman, K. L., 1973: A time-dependent model of the upper ocean. J. Phys. Oceanogr., 3, 173-184.
- \_\_\_\_\_, and M. Miyake, 1973: Upper layer modification at ocean station PAPA: Observations and simulation. J. Phys. Oceanogr., 3, 185-196.
- Duncan, T. M., 1973: Data handling features of the Electra Data Management System. Atmos. Tech., No. 2, 47-50.
- Dye, J. E., 1976: Comparisons of Electrostatic Disdrometer with Impactor Slides. J. Appl. Meteor., 15, 783-789.
- Eppley Laboratory, 1971: Instrumentation for the Measurement of the Components of Solar and Terrestrial Radiation. The Eppley Laboratory, Inc., 32 pp.
- Francisco, C. C., and D. J. Beaubien, 1965: "An Automatic Dew Point Hygrometer with Thermoelectric Cooling," Humidity and Moisture, Vol. I, 165-173.
- Fukuta, N., V. K. Saxena, and A. Gorove, 1974: Cloud Condensation Nuclei Spectrometer II: Measurements on the natural aerosol. Conference on Cloud Physics, Tuscon, Arizona, 361-367.
- Gill, A. E., and J. S. Turner, 1974: Mixing models for the seasonal thermocline. Norpax Highlights, Vol. 2, No. 5, Scripps Inst. of Oceanog., La Jolla, California, 9-12.
- Goodman, J. K., 1975: The Microstructure of California Coastal Fog and Stratus. Department of Meteorology, San Jose State University, 61 pp.
- Grams, G. W., 1974-75: Lidar: Some current uses and potential applications in the atmospheric sciences. Atmos. Tech., No. 6, 61-70.
- \_\_\_\_\_, and C. M. Wyman, 1972: Compact laser radar for remote atmospheric probing. J. Appl. Meteor., 11, 1108-1113.
- \_\_\_\_\_, E. M. Patterson, and C. M. Wyman, 1975: Airborne laser radar for mapping two-dimensional contours of aerosol concentration. Opt. and Quant. Elec., 7, 187-191.
- Kelley, N. D., 1973a: Electra Data Management System. Atmos. Tech., No. 1, 21-24.
- \_\_\_\_\_, 1973b: Meteorological uses of inertial navigation. Atmos. Tech., No. 1, 37-39.
- Kim, J.-W., 1976: A generalized bulk model of the oceanic mixed layer. J. Phys. Oceanog., (in press).

- Knollenberg, R. G., 1970: The optical array: An alternative to scattering or extinction for airborne particle size determination. J. Appl. Meteor., 9, 86-103.
- \_\_\_\_\_, 1972: Comparative liquid water content measurements of conventional instruments with an optical array spectrometer. J. Appl. Meteor., 11, 501-508.
- Krauss, E. B., 1968: What do we not know about the sea-surface wind stress. Bull. Am. Met. Soc., 49, 247-253.
- \_\_\_\_\_, and J. S. Turner, 1967: A one-dimensional model of the seasonal thermocline: II. The general theory and its consequences. Tellus, 19, 98-106.
- LeMone, M. A., and W. T. Pennell, 1976: The relationship of trade wind cumulus distribution to subcloud layer fluxes and structure. Mon. Wea. Rev., 104, 524-539.
- Lenschow, D. H., 1971: Vanes for sensing incidence angles of the air from an aircraft. J. Appl. Meteor., 10, 1339-1343.
- \_\_\_\_\_, 1972: The measurement of air velocity and temperature using the NCAR Buffalo aircraft measuring system. NCAR TN/EDD-74, National Center for Atmospheric Research, 39 pp.
- \_\_\_\_\_, 1973a: Two examples of planetary boundary layer modification over the Great Lakes. J. Atmos. Sci., 30, 568-581.
- \_\_\_\_\_, 1973b: Air sensing probes on the Buffalo. Atmos. Tech., No. 1, 40-42.
- \_\_\_\_\_, 1975: The use of aircraft for probing the atmospheric boundary layer. Atmos. Tech., No. 7, 44-49.
- \_\_\_\_\_, and W. T. Pennell, 1974: On the measurement of in-cloud and wet bulb temperatures from an aircraft. Mon. Wea. Rev., 102, 447-454.
- Leondes, C. T., 1970: Inertial navigation for aircraft. Sci. American, 222, 80-86.
- Lilly, D. K., 1968: Models of cloud-topped mixed layers under a strong inversion. Quart. J. Roy. Meteor. Soc., 94, 292-309.
- \_\_\_\_\_, and D. H. Lenschow, 1971: Aircraft Measurements of the atmospheric mesoscales using an inertial reference system. Fac. Atmos. Res., No. 19, 2-8.
- Miller, A., 1975: Project STABLE. Bull. Am. Met. Soc., 56, 52-55.

- \_\_\_\_\_, 1976: Wave Properties in the West Coast Inversion. San Jose State Meteorology Department, 95 pp.
- Neel, C. B., Jr., 1955: A heated-wire liquid-water content instrument and results of initial flight tests in icing conditions. Res. Memo. A54123, National Advisory Committee for Aeronautics.
- \_\_\_\_\_, and C. P. Steinmetz, 1952: The calculated and measured performance characteristics of a heated-wire liquid-water content meter for measuring icing severity. Tech. Note No. 2615, National Advisory Committee for Aeronautics.
- Neiburger, M., 1960: The relation of air mass structure to the field of motion over the Eastern North Pacific Ocean in summer. Tellus, 12, 31-40.
- \_\_\_\_\_, D. S. Johnson, and C.-W. Chien, 1961: Studies of the structure of the atmosphere over the Eastern Pacific Ocean in summer, I: The inversion over the Eastern North Pacific Ocean. Univ. Calif. Publ. Meteor., 1, No. 1.
- Niiler, P. P., 1975: Deepening of the wind-mixed layer. J. Mar. Res., 33, 405-422.
- Particle Measuring Systems, 1975: Standard Instrument Specifications, Pricing and Delivery. Particle Measuring Systems, 92 pp.
- \_\_\_\_\_, 1976: Forward Scattering Spectrometer Probe, PMS Model FSSP-100, Operating Manual. Particle Measuring Systems, 56 pp.
- Pennell, W. T., and M. A. LeMone, 1974: An experimental study of turbulence structure in the fair weather trade wind boundary layer. J. Atmos. Sci., 31, 1308-1323.
- Pollard, R. T., P. B. Rhines, and R. O. R. Y. Thompson, 1973: The deepening of the wind-mixed layer. Geophys. Fluid Dynamics, 3, 381-404.
- Riehl, H., T. C. Yeh, J. S. Malkus, and N. E. LaSeur, 1951: The northeast trade of the Pacific Ocean. Quart. J. Roy. Meteor. Soc., 77, 598-626.
- Ruskin, R. E., 1976: Liquid water content devices. Atmos. Tech., No. 8, 38-42.
- Saxena, V. K., and N. Fukuta, 1976: Field applications of a new cloud condensation nucleus spectrometer: Investigations of continental and maritime aerosols. International Cloud Physics Conference, Boulder, Colorado.
- Schubert, W. H., 1976: Experiments with Lilly's cloud-topped mixed layer model. J. Atmos. Sci., 33, 436-446.

- Telford, J. W., and P. B. Wagner, 1974: The measurement of horizontal air motion near clouds from aircraft. J. Atmos. Sci., 31, 2066-2080.
- Thomson, D. W., 1972: Airborne refractometer measurements. Fac. Atmos. Res., No. 20, 15-17.
- von Ficker, H., 1936: Die Passatinversion, Veroff. Meteor. Inst. Berlin, 1, 5ff.

BIBLIOGRAPHIC DATA SHEET		1. Report No.	2.	3. Recipient's Accession No.
4. Title and Subtitle			5. Report Date	
Design and Execution of the Marine Stratocumulus Experiment			September 1976	
7. Author(s)			8. Performing Organization Rept. No.	
Joseph S. Wakefield and Wayne H. Schubert			256	
9. Performing Organization Name and Address			10. Project/Task/Work Unit No.	
Department of Atmospheric Science Colorado State University Fort Collins, Colorado 80523			11. Contract/Grant No. (NSF) ATM 76-09370, OCD 74-21678 (NASA) GA 31588	
12. Sponsoring Organization Name and Address			13. Type of Report & Period Covered	
National Science Foundation National Aeronautics and Space Administration National Center for Atmospheric Research			14.	
15. Supplementary Notes				
16. Abstracts				
<p>The design and field phases of an observational program to study marine stratocumulus clouds using a single aircraft (NCAR Electra) are discussed. The basic theoretical framework for the design of the experiment was provided by Lilly's cloud-topped mixed layer model. This theory relates the model unknowns, which are cloud top height, cloud base height, mixed layer moist static energy, mixed layer total water content, and turbulent flux profiles of moist static energy and total water, to certain input parameters, which are sea surface temperature, surface wind speed, large-scale divergence, the temperature and moisture fields above cloud top, and the radiative divergence near cloud top. We attempted to measure all model unknowns and input parameters using the Electra instrumentation and user supplied instrumentation. Five flights off the California coast were made between 5 June and 17 June 1976, each flight lasting approximately six hours. Examples of some of the flight data are shown.</p>				
17. Key Words and Document Analysis. 17a. Descriptors				
<p>Marine Stratocumulus</p> <p>Stratus</p> <p>Stratocumulus</p> <p>Mixed layer</p>				
17b. Identifiers/Open-Ended Terms				
17c. COSATI Field/Group				
18. Availability Statement			19. Security Class (This Report)	21. No. of Pages
			UNCLASSIFIED	74
			20. Security Class (This Page)	22. Price
			UNCLASSIFIED	